Symmetric Jacobian for local Lyapunov exponents and Lyapunov stability analysis revisited

Franz Waldner[a], Rainer Klages[b*]

[a] *Physics Institute, University of Zurich ,Winterthurerstr. 190, CH-8057 Switzerland*

[b] *Queen Mary University of London, School of Mathematical Sciences, Mile End Road, London E1 4NS, UK*

[*] Corresponding author

-mail address: waldner@physik.uzh.ch; ef.waldner@swissonline.ch; r.klages@qmul.ac.uk

A B S T R A C T

The stability analysis introduced by Lyapunov and extended by Oseledec provides an excellent tool to describe the character of nonlinear *n*-dimensional flows by *n* global exponents if these flows are stationary in time. However, here we discuss two shortcomings: (a) The local exponents fail to indicate the origin of instability where trajectories start to diverge. Instead, their time evolution contains a much stronger chaos than the trajectories, which is only eliminated by integrating over a long time. Therefore, shorter time intervals cannot be characterized correctly, which would be essential to analyse changes of chaotic character as in transients. (b) Although Oseledec uses an *n* dimensional sphere around a point $\underline{x}$ to be transformed into an *n* dimensional ellipse in first order, this local ellipse has not yet been evaluated. The aim of this contribution is to eliminate these two shortcomings. Problem (a) disappears if the Oseledec method is replaced by a frame with a 'constraint' as performed by Rateitschak and Klages (RK) [Phys. Rev. E 65 036209 (2002)]. The reasons why this method is better will be illustrated by comparing different systems. In order to analyze shorter time intervals, integrals between consecutive Poincaré points will be evaluated. The local problem (b) will be solved analytically by introducing the `symmetric Jacobian for local Lyapunov exponents' and its orthogonal submatrix, which enable to search in the full phase space for extreme local separation exponents. These are close to the RK exponents but need no time integration of the RK frame. Finally, four sets of local exponents are compared: Oseledec frame, RK frame, symmetric Jacobian for local Lyapunov exponents and its orthogonal submatrix.

PACS: 05.45.Ac, 05.45.Pq

Keywords: Lyapunov exponents; stability analysis; dynamical instability; symmetric Jacobian for local Lyapunov exponents.

1. Introduction

Lyapunov exponents [1] are a well-established tool [2-9] to analyse the type of chaos displayed by a trajectory $\underline{x}(t)$ as a solution of a nonlinear n-dimensional equation in the phase space $\boldsymbol{R}\{\underline{x}\}$,

$$\mathrm{d}\underline{x} / \mathrm{d}t = \underline{X}(\underline{x}) \quad . \tag{1}$$

Their evaluation is based on proofs by Oseledec [2] that a vector $\underline{u}$ to any arbitrarily chosen neighbouring point of $\underline{x}$ (except the instantaneous direction along $\mathrm{d}\underline{x}$ as discussed later) will rotate to the direction of integrated extreme expansion. After an initial period, this local direction obtained through integrated rotation is an inherent feature of each point on the trajectory. Moreover, this local uniqueness applies to the set of all n directions of a frame orthogonalised subsequently after each time step. The integration for infinite time $t \rightarrow \infty$ of the corresponding local exponents results in a set of n Lyapunov exponents assessing the character of chaos in terms of dynamical instability of the given dynamical system.

The fact that an initial frame rotates after a short time to a locally unique orientation has fascinated many authors. This fascination includes the corresponding local exponents which has, probably, prevented one to ask: Is the local exponent leading to the largest Lyapunov exponent already locally assessing the strongest expansion, i.e. the strongest divergence of neighbouring trajectories, thus identifying the places where trajectories diverge, the origin of instability and chaos? A quick look at this exponent for the Lorenz model reveals that this is not the case resulting in misleading results for shorter time intervals.

The origin of this discrepancy is inherent to the idea of Lyapunov and Oseledec: They considered a sphere of neighbouring points. Each vector $\underline{u}$ not orthogonal to the direction $\mathrm{d}\underline{x}$ of the trajectory contains a component parallel to $\mathrm{d}\underline{x}$. This component measures only the expansion along the trajectory, hence the acceleration, which is not connected to instability. Only the component orthogonal to $\mathrm{d}\underline{x}$ analyzes the change of the distance to neighbouring trajectories and can indicate where trajectories start to diverge. This feature is obscured by the admixing of the acceleration. Since in many cases the average acceleration is zero, the integration for long times cancels this contribution, thus only the value for divergence remains.

These shortcomings can be avoided using a method introduced by Rateitschak and Klages (RK) [10], which was rediscovered independently by Grond et al. [11]: Select as an initial direction $\underline{u}$ the direction of $\mathrm{d}\underline{x}$, thus $\underline{u}$ is parallel to the trajectory. Certainly, this direction will remain parallel to the trajectory for all times. The integral of the corresponding exponent will only describe the average acceleration which for many cases

is zero, i.e., if the flow remains bounded and does neither shrink nor blow up. This exponent is not related to the problem of instability. However, all remaining directions of the initial frame, subsequently orthogonalised and their rotation integrated, are describing the divergence of neighbouring trajectories. Their corresponding exponents are the important numbers for analysing the nature of chaos. After an initial period much shorter than for the Oseledec method these directions are unique to the point $\underline{x}(t)$. The first in the orthogonalizing procedure of the corresponding local exponents is the largest one quantifying where trajectories diverge. Moreover, integrals for shorter time intervals analyse the chaotic character of the trajectories thus discriminating between intervals of strong and weak or no chaos.

This problem of finding coordinate systems in which trivial eigendirections are eliminated has already been addressed by Eckhardt and Wintgen in 1991 [12]. However, they focussed on periodic orbits in conservative two degree of freedom Hamiltonian systems for which they eliminated the two trivial neutral directions along the orbit and perpendicular to it on the energy shell by also requiring certain smoothness properties. Their Hamiltonian method was reviewed and further amended by Gaspard for calculating local Lyapunov exponents and local stretching rates [13]. Other numerical methods for computing local Lyapunov exponents and stretching rates have been proposed and tested in Refs. [10,11,14-16].

Similarly to Refs. [11,15], both Oseledec and RK methods will be illustrated for the Lorenz [17] and the Rössler model [18] by comparing them with each other and by also applying them to shorter time intervals for transient chaos. It is one of the main points of this contribution to show that the method using a set orthogonal to the flow is more adequate to describe the chaotic behaviour than the Oseledec method using general directions, thus explaining why Rateitschak and Klages [10] found much improved results introducing this method for complex chaotic behaviour. We also discuss similarities and differences between our refined stability analysis and the very recent concept of covariant Lyapunov vectors [16,19-23].

Our paper is organized as follows: In Section 2 we briefly review local Lyapunov exponents by motivating the definition of the symmetric Jacobian for local Lyapunov exponents. We then combine the latter concept with the idea of using coordinate frames orthogonal to the flow. This leads to a set of four different methods for defining local directions and stability exponents. In Sections 3 to 6 we compare the altogether four old and new methods with each other by applying them to numerically characterize chaos in the Lorenz and Roessler systems that is stationary in time. Sections 7 to 9 qualitatively explore similarities and differences of these concepts for transient chaos. Section 10 includes a brief discussion of similarities and differences between our method and the computation of so-called covariant Lyapunov vectors. There is also a

Supplement for this article, which contains a quantitative comparison of the different approaches, an assessment of local extreme divergence, and some remarks on norm dependence of local exponents. Conclusions are drawn in Section 11. An earlier, more detailed version of this paper is available as Ref. [24].

2. Stability analysis of a dynamical system at a point $\underline{x}$ in phase space

2.1 Geometric interpretation of local expansion

In order to understand the definition and use of what later on we call ``symmetric Jacobian for local Lyapunov exponents' we first briefly review the origins of Lyapunov instability analysis. For the following considerations we assume that our dynamical system is ergodic.

(i) The basic idea of Lyapunov exponents is to follow the evolution of points close to the points $\underline{x}(t)$ on a trajectory. First, these neighbouring points are chosen on an n-dimensional sphere around the starting point $\underline{x}(t_o)$. Then this sphere is continuously deformed during the time evolution. After a sufficiently long integration time τ this deformed object is analysed. From the largest expansion direction the largest Lyapunov exponent is evaluated. Starting with the direction of this largest expansion, further orthogonal directions are used to measure their expansions, which complete the set of n Lyapunov exponents. In practice, this method has to be combined with renormalization of the different components.

(ii) In principle, the evolution of the deformation should be numerically computed for a very large number of points on the initial sphere, a tremendous task even for large computers.

(iii) However, the works of Lyapunov [1] and Oseledec [2] propose a well-established, much less elaborate method: Arbitrarily defined at the start, choose an orthogonal frame of only n directions, follow their evolution - orthogonalised always in the same order by the Gram-Schmidt orthonormalisation method before each integration step - and measure their expansion, thus disregarding their rotation. The Lyapunov exponents are then obtained as the averages of the logarithms of these expansions. Note that only more recently it was shown that the basis of vectors defined by Benettin's method [3] converges to the eigenvectors of Oseledec [25].

It would be interesting to test to which extent (iii) corresponds to (i) in case (ii) could be treated with less numerical effort. It is the aim of this section to propose a simpler method. Before using the computer for

doing (ii), let's go back to the 19th century of Jacobi. Jacobi [26] used only the first derivative to define his matrix $\boldsymbol{J}$ at a point $\underline{x}$,

$$\boldsymbol{J}(\underline{x}) = \mathrm{d}\underline{X} / \mathrm{d}\underline{x} \quad . \tag{2}$$

He realised that the sum of the diagonal elements of $\boldsymbol{J}$ measures the local rate of change of the volume of a sphere around $\underline{x}$ in the limit of infinitesimally small radius. However, nothing has been said then about the deformation of this sphere. Although finally global quantities should be evaluated, we will first consider 'instantaneous local' quantities defined by the deformation between a fixed time t and $t+\mathrm{d}t$, starting as a sphere at t.

Applying this method to the deformed sphere, what is the first approximation? This has been shown already by Farmer et al. [4] with a picture of an ellipse in two dimensions. Green and Kim [7] describe a general ellipsoid for n dimensions, which is continuously deformed in time but remains always an ellipsoid. The problem (i) is then solved by using the n principal axes and their corresponding expansions for the final ellipsoid. Obviously, these principal axes are orthogonal in accord with (iii), since the ellipsoid has inversion symmetry. An n-dimensional ellipsoid is described by a symmetric n x n matrix $\boldsymbol{E}$, with orthogonal eigenvectors as principal axes and real eigenvalues, and is determined by $n(n+1)/2$ parameters. At this point it seems worthwhile to note that $\boldsymbol{E}$ yields the radius for the infinite number of possible directions as diagonal elements $(\boldsymbol{E}_U)_{ii}$ of $\boldsymbol{E}_U$, after transforming to a new coordinate system with the unitary matrix $\boldsymbol{U}$ and its transpose $\boldsymbol{U}^T$ as $\boldsymbol{E}_U=\boldsymbol{U}^T\,\boldsymbol{E}\,\boldsymbol{U}$. The matrix $\boldsymbol{E}$ has the same size as $\boldsymbol{J}$. However, $\boldsymbol{J}$ is in principle not symmetric causing complex eigenvalues and non-orthogonal complex eigenvectors. Furthermore, its diagonal elements are connected with the rate of change of the radius of a sphere, not with the radius of the ellipsoid described by $\boldsymbol{E}$. Therefore, why not try to symmetrise $\boldsymbol{J}$ while keeping the diagonal elements by defining a symmetric matrix $\boldsymbol{S} = ½\,(\boldsymbol{J} + \boldsymbol{J}^T)$ with orthogonal eigenvectors and real eigenvalues in order to describe the rates of change of the radii when the sphere is transformed in first order into an ellipsoid? This paper aims to convince the reader that $\boldsymbol{S}$ is exactly describing in first order the 'instantaneous local rates of exponential stretching ratio' – in short 'local exponents' - for all possible directions, although only n^2 numbers are involved in $\boldsymbol{J}$.

The idea of using a symmetrised Jacobian has already been introduced earlier by Hoover et al. for simplifying the Lyapunov stability analysis in terms of a singular value decomposition [27], however, here

we exploit this symmetry using a different approach. Even earlier, it has also almost been found by Goldhirsch et al. [6] in their eq. (3.7) and by Greene and Kim [7] in their eqs. (26)-(28). The latter authors showed that their instantaneous local expansion exponents λ_U along any orthogonal set of directions $\boldsymbol{U}$ are given by the diagonal elements $\boldsymbol{K}_{ii}$ of $\boldsymbol{K}=\boldsymbol{U}^T\,\boldsymbol{J}\,\boldsymbol{U}$ (note that in general $\boldsymbol{J}$ and $\boldsymbol{K}$ are not symmetric). Simply reduce this equation for only one direction $\underline{u}$ to the scalar product $\lambda_{\underline{u}}=(\underline{u},\boldsymbol{J}\underline{u})$. This form can be derived in a direct geometrical way providing probably one of the simplest approaches to define local Lyapunov exponents. The derivation is so short that it will be sketched here as follows:

Local expansion of a vector $\underline{u}$ to a neighbouring point of $\underline{x}(t)$ during a time interval Δt can be described in first order by using the Jacobian matrix $\boldsymbol{J}$ to

$$\underline{u}(t+\Delta t) = \underline{u}(t) + \boldsymbol{J}(t)\,\underline{u}(t)\,\Delta t \;=\; \underline{u}(t) + \Delta\underline{u} \quad , \tag{3}$$

where the new vector $\underline{u}(t+\Delta t)$ will have rotated and changed its length from d to $d+\Delta d$. If only the change Δd of the length is considered, the rotation can be eliminated by projecting $\Delta\underline{u}$ onto $\underline{u}$ by using the scalar product $\Delta d \approx (\underline{u}\,,\,\boldsymbol{J}\underline{u})\,\Delta t/\,|\,\underline{u}\,|^2$ valid for $\Delta t\rightarrow 0$. With the stretching ratio $r = (d+\Delta d)\,/\,d = 1 + \Delta d/d$ the local exponent $\lambda_{\underline{u}}$ for the direction of $\underline{u}$ is found according to the form [7]

$$\lambda_{\underline{u}} = (1/\Delta t)\,\ln\,(r) \tag{4}$$

giving $\lambda_{\underline{u}} = (1/\Delta t)\,\ln\,(\,1 + \,\Delta d/d\,) = (1/\Delta t)\,\ln\,[\,1 + \,(\underline{u}\,,\,\boldsymbol{J}\underline{u})\,\Delta t\,/\,|\,\underline{u}\,|^2]$. Using $\ln(1+\alpha) \approx \alpha$ for $|\,\alpha\,| << 1$, the result is the scalar product

$$\lambda_{\underline{u}} = (\underline{u}\,,\,\boldsymbol{J}\underline{u}) \tag{5}$$

if the vector $\underline{u}$ has been normalized to unity. Now note that in the scalar product $(\underline{u},\boldsymbol{J}\underline{u})$ the values $\boldsymbol{J}_{ik}$ and $\boldsymbol{J}_{ki}$ appear in pair sums $(\boldsymbol{J}_{ik} + \boldsymbol{J}_{ki})$. This symmetry is enforced by the special structure of the scalar product $(\underline{u},\boldsymbol{J}\underline{u})$: on both sides there occurs the same vector $\underline{u}$. Therefore, the same result is obtained for a symmetrised Jacobian matrix $\boldsymbol{S}$ constructed by adding the transpose $\boldsymbol{J}^T$,

$$\boldsymbol{S} = \tfrac{1}{2}\,(\boldsymbol{J} + \boldsymbol{J}^T) \tag{6}$$

with

$$\lambda_{\underline{u}} = (\underline{u}\,,\, \boldsymbol{S}\,\underline{u}) \quad . \tag{7}$$

Going now back to the above form $\boldsymbol{K}=\boldsymbol{U}^T\,\boldsymbol{J}\,\boldsymbol{U}$ of Green and Kim [7] and replacing there $\boldsymbol{J}$ by $\boldsymbol{S}$, the diagonal elements $\boldsymbol{T}_{ii}$ of the new matrix $\boldsymbol{T}=\boldsymbol{U}^T\,\boldsymbol{S}\,\boldsymbol{U}$ are equal to $\boldsymbol{K}_{ii}$. In contrast, this new $\boldsymbol{T}$ is a symmetric matrix corresponding to the symmetrised $\boldsymbol{K}$ with $\boldsymbol{T} = ½\,(\boldsymbol{K} + \boldsymbol{K}^T)$. Furthermore, the transformation of $\boldsymbol{J}$ with $\boldsymbol{K}=\boldsymbol{U}^T\,\boldsymbol{J}\,\boldsymbol{U}$ could be interpreted as transforming $\boldsymbol{J}$ into the new reference system $\boldsymbol{U}$ and the result might be denoted by $\boldsymbol{J}_U$. Similarly, $\boldsymbol{T} =\boldsymbol{U}^T\,\boldsymbol{S}\,\boldsymbol{U}$ transforms $\boldsymbol{S}$ into $\boldsymbol{S}_U= \boldsymbol{U}^T\,\boldsymbol{S}\,\boldsymbol{U}$ with its diagonal elements $(\boldsymbol{S}_U)_{ii}$ as instantaneous local exponents in the $\boldsymbol{U}$ directions. Thus $\boldsymbol{S}$ is the generating form containing all deformations of the ellipsoid and will be called `symmetric Jacobian for local Lyapunov exponents' (not to be confused with ‘deformed ellipsoid $\boldsymbol{E}$' which describes directly the radii, not the rates of their changes). In other words, $\boldsymbol{S}$ is the generator for Lyapunov exponents of all directions in the full tangent space

We remark that introducing the matrix $\boldsymbol{S}$ for assessing Lyapunov instability fully complies with standard textbook approaches of defining Lyapunov exponents [8,13]. Here the exponents are given in terms of the norm of the fundamental matrix $\boldsymbol{M}$, which describes the evolution of tangent space vectors. The exact solution for $\boldsymbol{M}$ is an exponential, see, e.g., eq. (1.14) of Ref. [13]. Simply expand this exponential to linear order in time and work out the corresponding product $\boldsymbol{M}^T\boldsymbol{M}$ in eq. (1.16) of [13], which defines the Lyapunov exponents. This yields the exponents in terms of the matrix $\boldsymbol{S}$. Note that using the symmetry argument is a consequence of the reduction of the deformation to lowest order. In reality, the deformations are more complicated than being captured in lowest order. As a by-product, the largest eigenvalue of the main principal axis of $\boldsymbol{S}$ gives the extreme rate of expansion of the sphere, its eigenvectors rarely being parallel to any of the frames in Section 1.

The above first step defines the instantaneous local deformation. The second step now consists of evaluating global quantities both for schemes (i) and (iii) above in order to test them in the long time limit. In both cases, global exponents are defined as final deformations after integrating all deformations during a time interval $\tau=t_{final} - t_{initial}$ for $\tau\rightarrow\infty$.

Before going into further detail, two important questions have to be answered: Have `deformations of previous deformations' to be evaluated? And have rotations of the ellipsoids to be incorporated? The answers

to both questions are illustrated in figure 1 of Benettin et al. [3]: After each time step the new deformation does not account for the previous deformation, that is, the deformation of the previous deformation is of higher order and can be neglected. Thus instantaneous local quantities can be averaged if integration is replaced by small but finite time steps as in numerical work. As far as rotation is concerned, each new start in Benettin's figure 1 is from a rotated direction. Since $\boldsymbol{S}$ does not contain any information about the rotation, it has to be incorporated separately, thus at each time step the transformed $\boldsymbol{S}_U(t) = \boldsymbol{U}^T(t)\ \boldsymbol{S}\ (t)\ \boldsymbol{U}(t)$ has to be evaluated. Note that for $\boldsymbol{U}(t)$ any of the two orthonormalised frames of section 1.1 could be used. Furthermore, note that $\boldsymbol{S}_U(t)$ has usually non-zero off-diagonal elements implying that the diagonal elements are no eigenvalues.

Now, on the basis of the new symmetric Jacobian for local Lyapunov exponents $\boldsymbol{S}$, differences between (i) and (iii) will be described. The evaluation according to (i) has to be done in two steps: First, average all local matrices $\boldsymbol{S}_U(t)$ along a typical trajectory. Obviously, each of the n^2 elements of $\boldsymbol{S}_U(t)$ has to be averaged separately. Hence this averaging results in a final symmetric matrix $\boldsymbol{S}_{final}$. In a second step, only for this final matrix $\boldsymbol{S}_{final}$ the eigenvalues and the eigenvectors have to be evaluated corresponding to global Lyapunov exponents and Lyapunov directions, respectively.

The recipe for performing (iii) is much simpler: The averages of the n diagonal elements $(\boldsymbol{S}_U)_{ii}(t)$ of the local matrix $\boldsymbol{S}_U(t)$ along a typical trajectory are the global Lyapunov exponents. Again obviously, each of the n diagonal elements of $(\boldsymbol{S}_U)_{ii}(t)$ has to be averaged separately. Comparing both methods, the results of (iii) are already incorporated in the final matrix $\boldsymbol{S}_{final}$ as diagonal elements. Hence, to test the equivalence between (i) and (iii) it is sufficient to compare the values of the diagonal elements of $\boldsymbol{S}_{final}$ with its eigenvalues. This test has been performed numerically for Lorenz chaos. There are small but distinct deviations for the free running rotation of Oseledec. The test is successful for the constraint rotation of RK.

So far the literature has mainly focused on local and global Lyapunov exponents. Both quantities have been defined above within a new approach, and tests of this concept will be described later on in this paper. But previous concepts of Lyapunov instability are only appropriate for chaos in a stationary regime, where a trajectory does not change its character in time. They are not suitable to analyse transients, crises, or continuous changes of parameters in time in equations of motion. However, an adequate method is easy to find: Instead of only considering ‘global quantities’ defined for an infinite interval of time τ, try a series of successive finite time intervals τ_n, each starting at t_n and ending at t_{n+1}. It is essential to define the successive times t_n such that the resulting data correspond to the character of the trajectory. The method (iii) based on a

series of finite intervals is then successfully applied to transient Lorenz chaos. It distinguishes well between an initial period of weak chaos, an intermediate period of strong chaos, and a final spiralling onto a stable fixed point. Also here the RK frame is superior to the Oseledec frame. As a by-product, each instantaneous local subspace $\boldsymbol{S}^{\perp(2\ldots n)}$ orthogonal to the flow - to be calculated at any point $\underline{x}$ of the phase space $\boldsymbol{R}\{\underline{x}\}$ – has n-1 eigenvalues. The largest eigenvalue within this subspace accounts for the extreme rate of divergence between neighbouring trajectories, not obscured by partial acceleration. This yields a novel indicator for extreme local divergence, which can be used to find 'hot spots' of maximum local dynamical instability in the whole phase space. These applications demonstrate that the new 'symmetric Jacobian for local Lyapunov exponents' is a powerful tool, which furthermore opens a pedestrian approach to defining both local and global Lyapunov exponents.

2.2 Comparison of four types of instantaneous local exponents

The novelty of this work is that it compares four types of local directions and exponents with each other. The first two are strictly local to $\underline{x}$. They use only the knowledge of the local Jacobian $\boldsymbol{J}$ and the value of $\mathrm{d}\underline{x}$, there is no need to evaluate any trajectory by integration:

1. The instantaneous local extreme expansion exponent of a local sphere and its corresponding direction are found as the largest eigenvalue and eigenvector of $\boldsymbol{S}$. Note that this yields the maximal possible value of the exponent for all four different methods, and the direction of this maximal deformation is rarely parallel to the direction obtained by the other three methods.

2. The extreme exponent for the instantaneous local divergence of neighbouring trajectories measured orthogonal to $\mathrm{d}\underline{x}$ and its direction are found as the largest eigenvalue and eigenvector of the subset $\boldsymbol{S}^{\perp}$. Note that this exponent is the maximal possible value of the largest exponent for divergence in what we will call the $\boldsymbol{W}$ frame of RK as described in method 4 below.

The other two types are evaluated by method (iii) and need integrations both of a trajectory and the directions of the frames.

3. The standard method of Oseledec (O) with an integrated free running frame called $\boldsymbol{V}$ frame produces n instantaneous local exponents and directions. The first exponent is associated with a covariant Lyapunov vector, as is further explained in Section 10, and is thus time reversal invariant; the remaining exponents are not time-reversal invariant.

4. The method of RK using an integrated $\boldsymbol{W}$ frame, where the first direction is always constrained to be parallel to d$\underline{x}$ thus assessing the instantaneous local acceleration parallel to d$\underline{x}$ (needs no integration). The remaining instantaneous local exponents are orthogonal to d$\underline{x}$ describing the divergence of neighbouring trajectories, with their corresponding directions found by integration of the $\boldsymbol{W}$ frame. Only the exponent corresponding to the flow direction is time-reversal invariant, because it is again associated with a covariant Lyapunov vector, see Section 10 for details; the remaining exponents are not time-reversal invariant.

These four different types of exponents are computed for two different paradigmatic chaotic dynamical systems, the Lorenz model [17], $dx/dt=\sigma(y-x)$; $dy/dt=\rho x-y-xz$; $dz/dt=bz-xy$ with control parameters (σ, ρ, b), and the Rössler model [18], $dx_1/dt = -x_1-x_3$; $dx_2/dt = x_1 + 0.25\ x_2 + x_4$; $dx_3/dt = 3 + x_1 x_3$; $dx_4/dt = -0.5\ x_3 + 0.05\ x_4$. The computations were performed numerically by using a higher order Runge-Kutta algorithm. The time steps and the integration times have been varied in order to check for the convergence of the results. The rotations of the different frames were evaluated with eq. (3), only for the first constrained vector of RK the flow direction of $\underline{X}(t)$ of eq. (1) was incorporated as proposed by RK. The Gram-Schmidt procedure was used for orthogonalising the frames.

2.3 The symmetric Jacobian for local Lyapunov exponents

A local n dimensional sphere around a point $\underline{x}$ of eq. (1) will be rotated and deformed after a time interval Δt into a complicated geometrical object. Only in linear approximation can its form be described by a symmetric n dimensional ellipsoid with orthogonal principal axes of the principal deformation exponents. Here, a straightforward simple way to find this ellipsoid will be described: The expansion exponent $\lambda_{\underline{u}}$ in any direction $\underline{u}$ is found by the scalar product ($\underline{u}$,$\boldsymbol{S}\underline{u}$), see eq. (7). Defining an orthonormal set $\boldsymbol{U}$ and its transpose $\boldsymbol{U}^T$, the transformed matrix $\boldsymbol{S}_U= \boldsymbol{U}^T\boldsymbol{S}\boldsymbol{U}$ can be evaluated. It is now important to note that the scalar product of eq. (7) implies that only the diagonal elements $(\boldsymbol{S}_U)_{ii}$ are equal to the local expansion exponents λ_i corresponding to the n orthogonal normalised directions $\underline{u}_i$ in $\boldsymbol{U}$. Note further that the off-diagonal elements $(\boldsymbol{S}_U)_{ik}$ with $i\neq k$ can have any non-zero value.

Let us first consider the special case that all off-diagonal elements $(\boldsymbol{S}_U)_{ik}$ with $i\neq k$ are zero. In this case, the diagonal elements $(\boldsymbol{S}_U)_{ii}= \lambda_i$ could be eigenvalues of $\boldsymbol{S}$. Since $\boldsymbol{S}$ is by definition symmetric, its eigenvalues α_i are real and the corresponding eigenvectors $\underline{a}_i$ are both real and orthogonal. It is then obvious from eq. (7) that the eigenvalues α_i can indeed be local expansion exponents. By expanding the arbitrary vector $\underline{u}$ in eq.(7)

into the basis of eigenvectors of $\boldsymbol{S}$, in complete analogy to the expectation value problem of a quantum mechanical operator [28], one concludes that the eigenvalues α_i are the extreme local expansion exponents, denoted by $\lambda_i^{(e)}$. This implies that the eigenvectors $\underline{a}_i$ correspond to the extreme vectors $\underline{u}_i^{(e)}$ of $\boldsymbol{U}^{(e)}$, which are orthogonal by definition. They transform the matrix $\boldsymbol{S}$ into its diagonal eigenvalue form $\boldsymbol{S}_{diag}=(\boldsymbol{U}^{(e)})^T \boldsymbol{S}\, \boldsymbol{U}^{(e)}$. The vectors $\underline{u}_i^{(e)}$ thus define the principal axes of the ellipsoid into which the local sphere is deformed.

Note that in the general case of arbitrary directions of $\boldsymbol{U}$ the corresponding local expansions exponents $\lambda_i=(\boldsymbol{S}_U)_{ii}$ are not eigenvalues of $\boldsymbol{S}$. In summary, according to eq. (7) the matrix $\boldsymbol{S}$ can be considered as the generator of deformations in all possible local directions including the principal axes which yield the extreme values [29]. It is therefore justified to call $\boldsymbol{S}$ the n-dimensional 'symmetric Jacobian for local Lyapunov exponents'. Note that $\boldsymbol{S}$ does not describe the deformed sphere. It accounts for the rate of expansion (positive values) or contraction (negative values) in any direction. Hence, this symmetric Jacobian can have values of both signs.

It will be convenient to order the exponents α according to their values $\alpha_k > \alpha_{k+1}$, thus the largest first, and the eigenvectors $\underline{a}_k$, written as columns in the matrix $\boldsymbol{A}_{\underline{x}}$ accordingly, its components expressed in the frame of $\boldsymbol{R}\{\underline{x}\}$. The symmetric Jacobian for local Lyapunov exponents can be written as a symmetric n dimensional tensor $\boldsymbol{T}$, its explicit form depending on the frame of reference. The simplest way is in the local frame of principal axes, the matrix $\boldsymbol{T}_{diag}$ with only the exponents α_k in the diagonal. Its trace as the sum of the exponents is clearly the rate of change of the volume of the sphere around $\underline{x}$. The more convenient form $\boldsymbol{T}_{\underline{x}}$ would be expressed in the reference frame of $\boldsymbol{R}\{\underline{x}\}$, to be found by back transformation, resulting, obviously, in the form of $\boldsymbol{S}$ expressed usually in the reference frame of $\boldsymbol{R}\{\underline{x}\}$, with the trace unchanged as the rate of change of the volume,

$$\boldsymbol{T}_{\underline{x}} = \boldsymbol{A}_{\underline{x}} \boldsymbol{T}_{diag} \boldsymbol{A}_{\underline{x}}^T = \boldsymbol{S}_{\underline{x}} \quad . \tag{8}$$

An alternative frame of reference will be described in the next section.

2.4 The orthogonal reduced symmetric Jacobian $S^{\perp(2,\ldots n)}$ for divergence

Although the symmetric Jacobian for local Lyapunov exponents contains all local information about neighbouring points, it is essential to find the principal exponents and their directions orthogonal to the flow. Only these directions indicate true divergence, because they are not disturbed by partial acceleration.

First the reason will be explained why these directions are important. Then an arbitrary local frame of reference is introduced serving to find the local frame of extreme divergence. The ellipsoid is transformed into this frame. After its truncation to the n-1 dimensional subspace orthogonal to the flow $\mathrm{d}\underline{x}$, the new extreme exponents and principal directions are found by solving the n-1 dimensional eigenvalue problem. Although these procedures are straightforward, the matrix operations will be described in more detail in order to facilitate their implementation in programs for Lyapunov exponents.

2.4.1 The mixing of divergence and acceleration

The symmetric Jacobian tensor will be described now by $\boldsymbol{S}_{\underline{x}}(\underline{x})$ at the point $\underline{x}$, the subscript denotes that the matrix is written in the coordinate system $\boldsymbol{R}\{\underline{x}\}$. $\boldsymbol{S}_{\underline{x}}(\underline{x})$ describes the rate of stretching along all possible directions $\underline{u}$ to a neighbouring point of any of the points $\underline{x}$ of the phase space without the need to execute any integration of eq. (1). Whereas most of these points belong to a neighbouring trajectory, there is one point exactly on the trajectory through $\underline{x}$. This point is found for $\Delta t \to 0$ along the vector $\underline{X}$ of eq. (1) which describes the flow through $\underline{x}$. Defining a flow unit vector $\underline{f}_{\parallel} = \underline{X} / |\underline{X}|$, the corresponding expanding exponent $\varphi_{\parallel}$

$$\varphi_{\parallel} = (\underline{f}_{\parallel}, \boldsymbol{S}_{\underline{x}} \underline{f}_{\parallel}) \tag{9}$$

does not describe any divergence of a neighbouring trajectory. Instead, it is the relative acceleration $(\mathrm{d}v/\mathrm{d}t)/v$ related only to the change of velocity v along the trajectory through $\underline{x}$ [7]. Hence, any vector $\underline{u}$ can be decomposed into a vector sum $\underline{u} = c_{\parallel}\underline{f}_{\parallel} + c_{\perp}\underline{g}_{\perp}$, where $\underline{g}_{\perp}$ is the appropriate unit vector in the space orthogonal to $\underline{f}_{\parallel}$. Therefore, $\underline{u}$ has its expansion exponent $\lambda_{\underline{u}}$ composed of the exponent $\varphi_{\parallel}$ related only to acceleration and $\lambda_{\perp \underline{g}}$ describing only the divergence of the neighbouring trajectory line in the $\underline{g}_{\perp}$ direction,

$$\lambda_{\underline{u}} = c_{\parallel}^2 (\underline{f}_{\parallel}, \boldsymbol{S}\underline{f}_{\parallel}) + c_{\perp}^2 (\underline{g}_{\perp}, \boldsymbol{S}\underline{g}_{\perp}) = c_{\parallel}^2 \varphi_{\parallel} + c_{\perp}^2 \lambda_{\perp \underline{g}} \tag{10}$$

2.4.2 Constructing the orthogonal reduced symmetric Jacobian for divergence

Hence, if the sole interest is to find locally the largest divergence of neighbouring trajectory lines, and not to be disturbed by interference with acceleration, the n-1 dimensional subspace orthogonal to the flow direction $\underline{f}_{\parallel}$ has to be constructed. This will be performed using an arbitrary local orthonormal set of reference $\boldsymbol{F}$ with the first column as the unit vector $\underline{f}_{\parallel}$. Then, construct the remaining n-1 vectors $\underline{f}_k$ by permutation of the components of $\underline{f}_{\parallel}$. Finally, use a Gram-Schmidt procedure to make the $\underline{f}_k$ orthogonal as columns of the matrix $\boldsymbol{F}_{\underline{x}}(\underline{x})$ expressed in the frame of reference $\boldsymbol{R}\{\underline{x}\}$ (denoted by subscript $_{\underline{x}}$) at the local point $\underline{x}$. The symmetric Jacobian for local Lyapunov exponents $\boldsymbol{S}_{\underline{x}}$ is transformed into the $\boldsymbol{F}$ frame by

$$\boldsymbol{S}_F = \boldsymbol{F}_{\underline{x}}^T \boldsymbol{S}_{\underline{x}} \boldsymbol{F}_{\underline{x}} \quad . \tag{11}$$

The first row and column of $\boldsymbol{S}_F$ describe the expansion along the flow. The remaining n-1 dimensional reduced square submatix $\boldsymbol{S}^{\perp(2,\ldots,n)}$ contains all expansions in the orthogonal subspace.

2.4.3 The principal local exponents for divergence

The reduced square submatix $\boldsymbol{S}^{\perp(2,\ldots,n)}$ is symmetric and has n-1 eigenvalues $\beta_{\perp k}$ and eigenvectors $\underline{b}_{\perp k}$ as the principal perpendicular local exponents and directions, respectively, again both to be ordered according to their values $\beta_{\perp k} > \beta_{\perp k+1}$, the largest first, and $\boldsymbol{B}$ is the n-1 dimensional matrix containing the ordered vectors $\underline{b}_{\perp}$ as columns. It is worthwhile to construct a local reference frame $\{\underline{h}\}$ as the matrix $\boldsymbol{H}$ with the first vector as the flow direction $\underline{f}_{\parallel}$ and the remaining directions as local perpendicular extreme expansion directions $\underline{b}_{\perp k}$. In the $\boldsymbol{F}$ frame, the first row and column are zero except $\boldsymbol{H}_{F11}$=1. The remaining submatrix is filled with the matrix $\boldsymbol{B}$. This frame $\boldsymbol{H}_F$ can be transformed into the reference frame of $\boldsymbol{R}\{\underline{x}\}$ by the arbitrary matrix $\boldsymbol{F}_{\underline{x}}$

$$\boldsymbol{H}_{\underline{x}} = \boldsymbol{F}_{\underline{x}} \boldsymbol{H}_F \quad . \tag{12}$$

Although the exponents $\beta_{\perp k}$ were evaluated already by solving the eigenvalue problem of the reduced submatrix $\boldsymbol{S}_{\perp}^{(2,\ldots n)}$, a general relation as a numerical control could be written using the frame matrix $\boldsymbol{H}_{\underline{x}}$ in a matrix product with the diagonal elements $(\ldots)_{ii}$ giving $\varphi_{\parallel}$ as the first, and $\beta_{\perp k=1,\ldots,n-1}$ as the remaining numbers

$$\varphi_{\parallel} = (\boldsymbol{H}_{\underline{x}}^{T}\ \boldsymbol{S}_{\underline{x}}\ \boldsymbol{H}_{\underline{x}})_{11} \qquad \beta_{\perp k=(1,\ldots,n-1)} = (\boldsymbol{H}_{\underline{x}}^{T}\ \boldsymbol{S}_{\underline{x}}\ \boldsymbol{H}_{\underline{x}})_{(k+1),(k+1)} \quad . \tag{13}$$

2.4.4 Exploring the whole phase space for extreme local divergence

Before a specific trajectory is evaluated, it seems worthwhile to explore the phase space by producing an n dimensional map of the principal exponent of local divergence $\beta_{\perp k=1}$ in order to find 'hot' regions of large divergence or 'cool' regions of missing divergence. However, applying this procedure to the Lorenz attractor the interpretation is not trivial; there are strong ‘hot’ and very ‘cool’ regions well outside the strange attractor. Examples will be given later. Moreover, changing the parameters in eq. (1) could result in a very different behaviour, more, stronger, less or no 'hot spots' in the whole phase space. To test this would be very elaborate by evaluating various trajectories. The procedure described here is much faster.

3. Exponents following a trajectory

A specific trajectory $\underline{x}(t)$ is found after choosing a starting point $\underline{x}_0 = \underline{x}(t=0)$ by integrating eq. (1) starting at $\underline{x}_0$. In the spirit of Lyapunov, n local exponents could be evaluated if a specific orthogonal set of directions is defined for each $\underline{x}(t)$. The average of these local exponents will for $t\rightarrow\infty$ lead to the Lyapunov exponents Λ_k characterizing the type of trajectory. Therefore, the problem of finding these local directions is essential. First, the well established method of Oseledec (O) without a constraint will be shortly described. Then the new method of Rateitschak and Klages (RK) with their constraint will be introduced. A comparison and a test will show later on that only the second method should be used, implying a fundamental change for the description of instability.

3.1The Oseledec (O) method for the local frame V

According to Oseledec [2], any arbitrarily chosen orthogonal frame $\boldsymbol{V}_0$ at the origin $\underline{x}_0$, rotated according to eq. (1), then orthogonalised and normalised after each time step Δt, will become a unique local frame $\boldsymbol{V}[\underline{x}(t)]$ for each point $\underline{x}(t)$ of the trajectory after an initial transient time τ_{transV}. The rotation can be evaluated by applying eq. (1) to neighbouring points or by using eq. (3) as proposed by Greene and Kim [7]. The idea is that the first direction, which is never adjusted by the orthogonalising process, will turn to the direction of strongest divergence from the trajectory, independently from its starting direction in $\boldsymbol{V}_0$. The instantaneous local expansion exponents λ_{Vk} can be found by eq. (5) or (7), and their averages will be the global Lyapunov exponents Λ_{Vk} for $t\rightarrow\infty$. The first exponent $\Lambda_{Vk=1}$ will be the largest.

At this point it is interesting to note that Moser and Meier [30] found in their numerical analysis of the angles of the $\boldsymbol{V}$ frame that the direction corresponding to the smallest ('most negative') local exponent is always nearly orthogonal to the flow. Small deviations are probably due to finite step integration and numerical limitations.

3.2The Rateitschak and Klages (RK) constraint frame W

Rateitschak and Klages (RK) [10] introduced a new concept for a local frame $\boldsymbol{W}$. The rotation can be made by eq. (3), and the first vector $\underline{w}_{k=1} = \underline{f}_{\|}$ is always set parallel to $\underline{X}/\left|\underline{X}\right|$. The remaining directions are then orthogonalised always in the same order. Also here, after a transient time τ_{transW} a unique frame $\boldsymbol{W}[\underline{x}(t)]$ for each point of the trajectory $\underline{x}(t)$ will be defined. The local expansion exponents λ_{Wk} can be found by eq. (5) or (7) by using $\boldsymbol{W}$ instead of $\boldsymbol{V}$, and their time averages will be the global exponents Λ_{Wk} for $t\rightarrow\infty$. Now, the first $\Lambda_{Wk=1} = \Lambda_{\|}$ will not be the largest. It has a different function: it measures the mean acceleration of the flow, which is zero for many chaotic models. The remaining $\Lambda_{Wk>1} = \Lambda_{\perp Wk}$ all describe only divergence of neighbouring trajectory lines, hence the second $\Lambda_{Wk=2}$ will be the largest.

A numerical test with the Lorenz model [17] confirmed that the third direction of the $\boldsymbol{V}$ frame is not only always nearly orthogonal to the flow [31], but also always nearly parallel to the third direction of the $\boldsymbol{W}$ frame, with deviations of the order of the deviations within the $\boldsymbol{V}$ frame.

3.3Comparing recovery times of Oseledec with Rateitschak and Klages

How fast does an arbitrarily chosen frame approach the locally unique frame directions, described by a transient time $\tau_{transient}$? This question is analysed in the Lorenz system by measuring the recovery time $\tau_{recover}$ of a suitably rotated frame. The test starts with a frame $\boldsymbol{V}$ at time t_0. At a time $t_1 >> \tau_{transient}$ a new frame $\boldsymbol{V}_{rot}(t_1)$ is constructed, which is rotated by 90 degrees with respect to $\boldsymbol{V}(t_1)$. Both frames are integrated in time, and the difference of the angles between the maximal expansion direction of the flipped $\boldsymbol{V}_{rot}(t)$ and the unflipped $\boldsymbol{V}(t)$ are plotted in Fig. 1 as a function of time t. Clearly, the recovery time $\tau_{recover}$ is much longer for O (top) than for RK (bottom). For RK, the direction of the flow is obviously not rotated at t_1 Therefore, only n-1 directions have to readjust. These recovery times $\tau_{recover}$ are an indication for the transient times τ_{trans} after t_0. In addition, it seems worthwhile to note that the exponent of the acceleration of the flow has zero recovery time, since its direction $\underline{X}/|\underline{X}|$ is the local value of eq. (1) for each point $\underline{x}$ of the phase space.

We remark that here this test was only performed for a low-dimensional dynamical system living in n=3 dimensions, where only two directions have to be adjusted in the orthogonal subspace. We suspect that in systems of larger dimensionality the discrepancy between the O and the RK method might be less profound. However, in any case the orientation of the first O direction typically has to change by large angles when the acceleration changes sign. But this change can only be done in small steps according to eq. (3). Therefore, there is a retarded reaction to rapid changes of the trajectory, such as at collisions [10]. Correspondingly, most of the n-1 remaining directions also have to move by large angles.

4. Comparing local directions and exponents as functions of time t

4.1 The four sets of directions and exponents

The following local sets of directions have been studied, each with n corresponding local exponents:

(1.1.) (A) The principal axes $\underline{a}$ in $\boldsymbol{A}$ of the 'full' symmetric Jacobian for local Lyapunov exponents $\boldsymbol{S}$, with local exponents α.

(1.2.) (B) The 'constrained' flow direction $\underline{f}_{\parallel}$ and the extreme divergence directions $\underline{b}_{\perp}$ of the 'reduced' Jacobian submatrix $\boldsymbol{S}_{\perp}^{(2,\ldots n)}$ (in contrast to the 'full' $\boldsymbol{S}$), both described by $\boldsymbol{H}$, with local exponents $\varphi_{\parallel}$ and $\beta_{\perp}$.

(2.1.) (V). The 'free' Oseledec (O) unique local frame $\boldsymbol{V}$ approximated after a transient time τ_{transV}, with local exponents λ_V.

(2.2.) (W) The ‘constrained’ Rateitschak and Klages (RK) unique local frame $\boldsymbol{W}$ approximated after a transient time τ_{transW}, with local exponents $\lambda_{\parallel W}= \varphi_{\parallel}$ and $\lambda_{\perp W}$.

The connections between these four local schemes are illustrated in Table 1.

We remark that in both the O and RK method the starting frames $\boldsymbol{V}_0$ and $\boldsymbol{W}_0$ are ambiguous. This ambiguity can be removed if the corresponding local frame defined by the symmetric Jacobian for local Lyapunov exponents is used. For the Oseledec frame the set $\boldsymbol{A}_{\underline{x}}$ refers to the principal deformation directions. For RK the frame $\boldsymbol{H}_{\underline{x}}$ has as a first vector the flow direction, the remaining ones are the local extreme directions of orthogonal divergence. For RK this setting shortens the transient time until the $\boldsymbol{W}_{\underline{x}}$ frame is close to the unique local frame.

4.2 Comparing the local exponents as functions of time t

The Lorenz model will be used to study local exponents as functions of time *t*. Fig. 2 (bottom) shows the *x* component as a function of time for a short time interval. Above, local exponents are displayed for the same time interval, the left side for the ‘free’ ‘full’ case, the right side for the ‘constrained’ ‘reduced’ case (see Table 1). For the ‘full’ case, Fig. 2 (left, top) plots the first ‘free’ exponent λ_{V1} together with the main principal exponent α_1 (fine line) as the local extreme value. The first exponent λ_{V1} is not at all times the largest and rarely has the extreme possible value of α_1. The difference (λ_{V1}- α_1), (left side, second row) has no relation to the *x* component (bottom). The third row, left, displays the second ‘free’ exponent λ_{V2}, again with α_1 (fine line). Remember that for $t\rightarrow\infty$ the average of the first exponent is positive and the second average approaches zero. Both local exponents λ_{V1} and λ_{V2} are a mixing of divergence and acceleration.

For the ‘constrained’ case, Fig. 2 (right, top), which discriminates between divergence and acceleration, shows the main principal exponent orthogonal to the flow $\beta_{\perp 1,}$ thus indicating the possible maximum of divergence. The first exponent for divergence $\lambda_{\perp W1}$ is very close to that maximum $\beta_{\perp k}$, with the small difference ($\lambda_{\perp W1}$- $\beta_{\perp}$) displayed below, related to the small deviation of the relative directions. However, the exponent for the local acceleration $\lambda_{\parallel W}= \varphi_{\parallel}$ of Fig. 2 right, third row, can have values nearly twice as large as the exponent $\lambda_{\perp W1}$ for divergence, but clearly never exceeds the main principal ‘full’ exponent α_1 (fine line). Comparing the left with the right hand side of Fig. 2, it seems obvious that the right hand side has a simpler structure and more resemblance with the structure of the *x* component than the left hand side. This

discrepancy is analysed in detail in Supplement A by suggesting a novel statistical test, resulting in a 'figure of merit' of about 1:100 in favour of RK.

5. Local exponents as functions of phase space $\boldsymbol{R}\{\underline{x}\}$ vs. x component

The temporal behaviour of the four local exponents has been extensively discussed in the previous sections. For a better understanding it seems worthwhile to explore their behaviour in the phase space $\boldsymbol{R}\{\underline{x}\}$. The directions of the Oseledec $\boldsymbol{V}$-frame were already shown in 3-D plots and discussed by Wolf et al. [5] and Green and Kim [7] for a short part of the Lorenz trajectory. Here, longer parts of trajectories changing the loop several times will be displayed

5.1 Lorenz local frame angles as a function of the x component

Figure 3 (top left) shows the angle of the first vector $\underline{v}_1$ of the 'free' $\boldsymbol{V}$ frame relative to the flow direction $\underline{f}_\parallel$ as a function of the x component. Clearly, this angle has a wide spread between 0 and 180 degrees. In both these extreme cases the exponent has a strong admixing of acceleration. In contrast, the first vector $\underline{w}^\perp{}_1$ of the 'constrained' $\boldsymbol{W}$ frame for divergence is by definition always orthogonal to the flow direction. In Fig 3 (top right) the angle of this direction $\underline{w}^\perp{}_1$ within the orthogonal plane relative to the direction $\underline{b}^\perp{}_1$ of the extreme divergence exponent $\beta^\perp{}_1$ is shown to be always small as a function of the x component with a range between -16 to 8 degrees. Therefore, the values of the divergence exponent $\lambda^\perp{}_{W1}$ are never far from the value of $\beta^\perp{}_1$.

5.3 Largest local exponents vs. local extreme divergence

Fig 3 (bottom right) shows the values of $\lambda^\perp{}_{W1}$ as a function of $\beta^\perp{}_1$ with the straight diagonal indicating the limit $\lambda^\perp{}_{W1} = \beta^\perp{}_1$. A similar diagonal $\lambda^\perp{}_{V1} = \beta^\perp{}_1$ is plotted in Fig. 3 (bottom left), showing the first 'free' exponent λ_{V1} also as a function of $\beta^\perp{}_1$. All the excess on the left side as compared to the right side has to be averaged out during integration in time t to finally describe only divergence.

At this point it is interesting to discuss how the algorithm to rotate the frames converges after a short transient already with respect to the direction that will yield the largest average exponent in the limit of long integration time: The first orthogonal vector $\underline{w}^\perp{}_1$ of the $\boldsymbol{W}$ frame oscillates around the local extreme direction

$\underline{b}_{\perp 1}$ with a small amplitude, see Fig. 3 (top right), thus finding the trajectory closest to the local extreme direction $\underline{b}_{\perp 1}$. Therefore, the local exponents $\lambda_{\perp W1}$ are not far below the corresponding extreme values $\beta_{\perp 1}$, see Fig. 2 (second row, right) and Fig. 3 (bottom right). Hence the average of the extreme exponent $\beta_{\perp 1}$ is a limit and not far from the global value of the largest orthogonal exponent $\lambda_{\perp W1}$, keeping in mind here that the extreme exponents $\beta_{\perp 1}$ are no Lyapunov exponents, only limits.

6. Local exponents as functions of phase space $R\{\underline{x}\}$ in the *yz* plane

Fig. 4 plots the projection of the trajectory onto the *yz*-plane when the local exponents exceed $c = 4$. The trajectory is plotted at equal time intervals in order to show the change of the velocity. The small circle denotes the maximal value. The left side displays the 'free' 'full' case, the right side the 'constrained' 'reduced' case (see table 1). The top rows show the strictly local exponents α_1 (general maximum) and $\beta_{\perp 1}$ (maximum of divergence only). The centre display the largest exponents of the integrated frames $\boldsymbol{V}$ and $\boldsymbol{W}$ as λ_{V1} (mixing divergence and acceleration) and $\lambda_{\perp W1}$ (divergence only), respectively. The bottom rows show the second exponents λ_{V2} (mixing acceleration and divergence) and $\lambda_{\parallel W} = \varphi_{\parallel}$ (acceleration only).

On the left side, only α_1 has clear cut borders at the limiting value of c, whereas centre and bottom exhibit a peculiar pattern. Furthermore, centre and bottom have regions where both exponents are above the limiting value. The right side of 'constrained' exponents shows a very different behaviour. Here the borders are clear functions of the phase space. Moreover, the top and centre are almost similar, the centre pattern only being slightly smaller. The centre and bottom patterns do not coincide. Finally, and most importantly, only the 'constrained' case right, top and centre, has large values where the real divergence of the two loops occurs. The discrepancy to the left side is easy to understand: Since acceleration is larger than divergence, and the first exponent λ_{V1} is a strong mixing of divergence and acceleration, the pattern bottom right $\lambda_{\parallel W} = \varphi_{\parallel}$ is easy to see in the pattern centre left λ_{V1}, and the maximum (small circle) is nearly at the same place. Hence, only the 'constrained' case seems to analyse directly the local chaotic behaviour.

The directions of both frames $\boldsymbol{V}$ and $\boldsymbol{W}$ are dependent on integration and not only on the location $\underline{x}$. This brings about a dependence on the former sections of the trajectory. Although the exponents are unique for each location $\underline{x}$, they are not simple functions of the phase space, since the former section of each location is different. The integration is a nonlinear procedure and, therefore, might have in itself a chaotic behaviour sensitive to small changes in the previous conditions. This implies a chaotic behaviour in addition to the

chaotic behaviour of the analysed chaotic trajectory, resulting in the fact that another trajectory nearby might have a very different local exponent caused by a tiny difference at earlier points of that trajectory. However, this additional complexity is very different for the two frames, dependent on their 'transient times' as a measure to 'forget' earlier sections of the trajectory and on the range of changing angles of the frames

Finally, and most importantly, only the 'constrained' case, right top and centre, displays large values where the separation between the two loops occurs, i.e., right at the point of instability that is important for making predictions whether a trajectory either cycles again on the same side or moves over to cycling on the other side.

A more detailed analysis of local instability by assessing local extreme divergence in phase space is reported in Supplement B of our paper. A discussion of the norm dependence of local exponents is contained in Supplement C.

7. The idea of integrating all directions of the local sphere

It seems worthwhile to recall here the basic idea behind the definition of Lyapunov exponents, which consists of integrating along a trajectory the subsequent deformations of the surface of a sphere, surrounding a given initial condition, along all direction in phase space. At the final time, the principal axes and eigenvalues of this deformed ellipsoid are considered to be the relevant characteristics of the problem, thus only n exponents are sufficient to describe the type of dynamical instability. It was proved by Oseledec that only the knowledge of the deformations of a frame of n orthogonal directions is necessary to find the relevant final parameters for these final axes. The evaluation of the deformation with the symmetric Jacobian $\boldsymbol{S}$ enables to test this established fact numerically.

7.1 The problem of subsequent rotation

It is straightforward to evaluate $\boldsymbol{S}[\underline{x}(t)]$ along a trajectory $\underline{x}(t)$. However, for calculating Lyapunov exponents from it the rotations of the directions after each time step dt still have to be eliminated. This important fact is not too obvious, since the expression $\boldsymbol{J}\underline{u}$ of eq. (3) implies elongation and rotation. However, in order to find instantaneous local exponents describing only elongation, the rotation must be projected out by using the scalar product of eq. (5). Moreover, because this scalar product has the same vector on both sides, it enforces the symmetrisation of the Jacobian matrix $\boldsymbol{J}$ in form of the symmetric Jacobian for local

Lyapunov exponents $\boldsymbol{S}$. Therefore, a rotation of $\boldsymbol{S}$ has to be performed after each time step dt along the trajectory. In principle, each direction should be rotated according to eq. (1) separately. However, as a crude oversimplification all orientations might be rotated equally according to the rotation of an n dimensional orthogonal frame evaluated with the equation of motion eq. (1). Since $\boldsymbol{S}$ does not contain any information about the rotation, this dynamics has to be incorporated separately, that is, at each time step the transformed $\boldsymbol{S}_U(t) = \boldsymbol{U}^T(t)\ \boldsymbol{S}\ (t)\ \boldsymbol{U}(t)$ has to be evaluated. Note that for $\boldsymbol{U}(t)$ only the RK frame is adequate, since the flow direction should be conserved by the rotation. The other orthogonal directions of RK determine the rotation around the flow direction. Furthermore, note that $\boldsymbol{S}_U(t)$ has usually non-zero off-diagonal elements implying that the diagonal elements are no eigenvalues.

Along these lines, transformations $\boldsymbol{S}$ into the frames $\boldsymbol{W}$ will be used. The average of values computed at discrete time steps will approximate the continuous time integration. Let the interval τ be divided into m parts Δt. With $\underline{x}_k = \underline{x}(t_0 + k\ \Delta t)$, the resulting arithmetic average $\boldsymbol{S}^{(\tau)}{}_W$ can be written as

$$\boldsymbol{S}^{(\tau)}{}_W = (1/\tau)\sum^{m}{}_{k=1}\ \boldsymbol{W}^T(\underline{x}_k)\ \boldsymbol{S}_x(\underline{x}_k)\ \boldsymbol{W}(\underline{x}_k) \qquad (14)$$

At the final time of the integration, the eigenvalues are evaluated and compared with the integrals of the exponents of the corresponding frames. For convenience, the eigenvalues will be ordered with the largest first for the principal axes of the averaged sums of the ellipsoids. In contrast, the averaged sums of the local exponents of the frames are ordered according to the order during the orthogonal normalization process, which might result in a reversed order, such that the value for the first exponent is smaller than for the second exponent.

7.2 Integration of all deformations for long times compared to global exponents and directions

The first test of comparing the three properties mentioned in the title of this subsection has been performed numerically for Lorenz chaos with parameters (σ, ρ, b)=(16, 40, 4). The test is successful by yielding the following values: global exponents of RK frame (1.37, 0.0001, -22.37); global eigenvalues of $\boldsymbol{S}_{final}$ (1.37, 0.0001, -22.37); global exponents of Oseledec (1.38, 0.002, -22.38). The deviations of the global eigenvectors of $\boldsymbol{S}_{final}$ relative to the RK frame $\boldsymbol{W}$ are less than one degree.

A similar test was performed when $\boldsymbol{S}$ was rotated by the O frame $\boldsymbol{V}$. The resulting values (1.59, 0.002, -22.59) for the global exponents $\boldsymbol{S}_{finalV}$ deviate from the global exponents of the O frame displayed above. Furthermore, the global directions of $\boldsymbol{S}_{finalV}$ are not parallel to the $\boldsymbol{V}$ frame.

The second test was performed for the 'hyperchaotic' Roessler model and was also successful yielding the following values: global exponents of RK frame (0.1157, 0.0205, 0.00095, -24.93); global eigenvalues of $\boldsymbol{S}_{final}$ (0.1157, 0.0203, 0.00069, -24.93); global exponents of Oseledec (0.1064, 0.0204, 0.0034, -24.92). The discrepancy regarding the first exponent of the O frame is probably caused by the retarded reorientation of the $\boldsymbol{V}$ frame after sharp and rapid spiking, which is typical for the Roessler model.

8. Why integrating exponents for short intervals between Poincaré points?

At the beginning of analysing chaos, the main interest was to find general numbers defined in the limit of $t\rightarrow\infty$, which presupposes stationary chaos that does not change its character in time. Later on, also chaotic motions were analysed where the strength of the chaotic behaviour was changing. Therefore, shorter time intervals were used. The large variation of the local exponents in time made the resulting numbers strongly dependent on the limits where the time intervals start and end. In order to test different methods, a chaotic behaviour with strongly changing character would be welcome. Such a 'transient' chaos will be described in the next subsection.

8.1 Two types of Lorenz chaos

Until now, the Lorenz chaos with parameters $(\sigma,\rho,\beta) = (16,40,4)$ was stationary with repelling unstable fixed points at $\underline{X}=0$, where trajectories starting nearby would spiral out, join the well-known double loop strange attractor and stay there in theory to infinity, in practice until the build-up of computing errors will be too high. A change of the parameter ρ *in* the Lorenz equation ($\mathrm{d}y/\mathrm{d}t = \rho x - y - x\,z$) from 40 to 28.165 replaces the unstable fixed points by attracting stable fixed points. Figure 5 bottom displays a peculiar 'transient' Lorenz trajectory starting with several loops on the right side with increasing radius, followed by a chaotic interval with loops on both sides, and a final decay spiralling on the left side to a stable fixed point.

8.2 Time intervals τ_p between Poincaré points for Lorenz trajectories

For the Lorenz chaos, integrating over one loop would be reasonable. Since there are no closed loops, well chosen Poincaré points will be used to define the start and end of a single loop. Poincaré points will be defined here when a trajectory is crossing a plane at $y=c_p$ 'from above', i.e. for decreasing values of y. The time interval τ_p is then defined between two consecutive Poincaré points. The plane parameter c_p is chosen at a level where the trajectories are about normal to the Poincaré plane. Figure 5 shows this plane as a line in the yz plot for the transient chaos (c_p=27.165) described above at the level of the attracting fixed points. The integration between Poincaré points is therefore performed over one loop. The results are shown in the next sections for the 'free' and 'constraint' case.

9. Poincaré integrals for 'transient' chaos with a sudden flip of the frames

*9.1 'Transient' with a sudden change of the frame: Oseledec **V** frame*

Figure 6 bottom shows the x component vs. time t for the 'transient' chaos described above. On top, the Poincaré integrals for the first two exponents of the ***V*** frame are plotted as o and +, respectively. The centre shows the angle of the first axis of the ***V*** frame relative to the flow direction. The frame starts with an arbitrary orientation. Then, at t = 7 the frame is suddenly rotated by 90 degrees. After this flip the reorientation to being nearly parallel to the flow is rather slow. During the short strongly chaotic regime the angle flips up and down. Long after the beginning of the spiralling down to the fixed point the angle reorients again between $t \approx 22$ and 27. This delayed motion causes a virtually chaotic pattern of the exponents, see top panel within approximately the same time interval, similar to the reaction at the beginning and after the flip. Furthermore, note that during the strong chaotic behaviour the integral of the second exponent is sometimes larger than the first exponent. Clearly, the Oseledec ***V*** frame has problems with delayed reorientation, which could give wrong exponents for finite time intervals.

9.2 'Transient' with a sudden change of the frame: RK ***W*** *frame*

Figure 7 bottom displays the x component of the same 'transient' chaos as in Fig. 6. Here the frame is also suddenly rotated by 90 degrees at t=7, as shown in the centre for the angle between the first orthogonal

direction of the ***W*** frame and the direction of the local orthogonal direction of extreme divergence. This flip changes the exponents only for the integral over one loop, as is shown on top for the second exponent, since the recovery time of the angle is small, and one direction along the flow remains fixed according to the definition of the 'constrained' ***W*** frame. This implies that the direction for the first exponent is independent of the orientation of the other directions of the ***W*** frame, so the flip at t=7 does not affect the first exponent $\lambda_{\parallel W}$, see + in Fig. 7 top panel.

9.3 Integrating the local extreme divergence exponents

It is also interesting to compare the RK Poincaré integrals with the integrals of the local extreme orthogonal exponents evaluated as largest eigenvalues of the local reduced Jacobian ellipsoid, see the dots above the symbols for the second exponent in Fig. 7. Since these integrals are for local exponents, they are independent of the orientation of any frame. Their values are always larger than the RK values, but they provide also an excellent description of the trajectory. They are small during the last part of the spiralling dynamics to a fixed point but still slightly positive there, which indicates chaotic behaviour. However, the negative integral of the exponent along the acceleration simultaneously indicates non-chaotic behaviour.

Hence the combination of both the local extreme exponent with the exponent along the acceleration leads already to a good estimate of the type of regime, chaotic or non-chaotic. Furthermore, both exponents have zero transient time, they are correct already at the staring time t_0. Since no frame ***V*** or ***W*** is needed, the ambiguity of a starting frame, their integration and their transient times are avoided.

Details about a quantitative comparison between the different exponents by suggesting a novel statistical test can be found in Supplement A.

10. Covariant Lyapunov vectors and refined Oseledec stability analysis

More recently, stability analysis of dynamical systems has focused on computing so-called covariant [19], respectively characteristic [20] Lyapunov vectors (CLVs) and corresponding exponents. CLVs are defined as being parallel to the locally expanding or contracting directions in phase space. They are thus mapped by the linearized dynamics into each other, which implies that they are time reversal invariant [19]. The numerical procedure for their computation, as outlined by Ginelli et al. [19], is nicely detailed in Ref. [21]; for a

pedagogical introduction see particularly Ref. [22]. Typically, CLVs are not orthogonal to each other. This is in contrast to the generic orthogonality of Oseledec vectors, which consequently are typically not time reversible. Hence these methods define two different bases of vectors for assessing dynamical instability, where CLVs are significantly harder to compute than Oseledec vectors. Both schemes have been compared to each other for a number of different dynamical systems [16,19-23]. While both bases lead to the same spectrum of global Lyapunov exponents [16], similarities and differences have been found in quantities such as Lyapunov modes [16,23].

By proposing a novel concept of assessing local stability in our article, we have refined the stability analysis of Oseledec along different lines [10-16] than proposed in terms of CLVs [16,19-23]. This has been achieved by defining a suitable symmetric Jacobian. However, combining this concept with the RK method yields an important cross-link to the covariant approach: By definition [19], the vector parallel to the flow is covariant, and this is exactly the one that is constrained by the RK method. One may thus wonder why the RK method is not by default implemented for computing CLVs. Secondly, computing the vector corresponding to the largest Lyapunov exponents by the conventional Oseledec method yields by definition [19] another CLV. Detailed information about the dynamics of these two CLVs is displayed in all figures of our article by comparing them to other (constrained, unconstrained) Lyapunov vectors and exponents. We remark in particular that computing the angle between the first and the second CLV, as we do for the Lorenz system in Fig. 3, cf. $\underline{v}_1$ for the first and $f_{\|}$ for the second CLV, has become a popular test for assessing the hyperbolic structure of a dynamical system [16,19,21].

However, in contrast to the CLV approach our method is designed to analyse equations of motion with a minimal effort in order to answer the simple question: Is the motion stable or not? This question was once important for experimentalists trying to simulate their measurements with appropriate equations of motion. A problem of the RK method is that up to now there are only numerical arguments available. Desirable would be a proof of the numerical observation in our models that the vector in the subspace orthogonal to the flow points to the direction with the largest global exponent after a short transient time.

In summary, our refined stability analysis provides a tool for rapidly assessing the stability of equations of motion with an emphasis on local features, short time integrations and transients. There is no proof similar to Oseledec for the subspace dynamics orthogonal to the flow, and the full approach does not preserve time reversal symmetry. Hence, it cannot and will not provide a substitution of the CLV method. Combining the

CLV approach with our method beyond constraining the flow vector, particularly in view of higher dimensional Lyapunov vectors, remains a challenge for future work.

11. Conclusions

In summary, the introduction of the symmetric Jacobian for local Lyapunov exponents and its submatrix orthogonal to the flow allows the direct determination of the principal exponents and of the extreme local exponent for diverging trajectories for every point in the phase space without the need to integrate along a specific trajectory to find the local 'Lyapunov directions' according to the procedure of Oseledec. Moreover, a fundamentally different approach evaluates the divergence of nearby trajectories by avoiding a mixing with local acceleration. This is performed by adding a simple constraint to the Oseledec frame as was already done in Refs. [10,11,15]: The first vector remains fixed along the flow direction d$\underline{x}$, and any further vectors are subsequently orthogonalised after each rotation, which implies that only the divergence and not any partial acceleration are assessed at every point on the trajectory. This avoids the additional complexity introduced by the Oseledec method, and the local exponents are in accord with the local divergence of the trajectories. The main problem of dynamical instability: *Remain neighbouring trajectories in a tube?* is thus solved. The largest exponent indicates locally already where trajectories diverge and where the origins of instability occur. Only the evaluation of the symmetric Jacobian for local Lyapunov exponents is treated analytically, the remaining conclusions are based on studying numerical examples. Hence, a formal revision of the original idea of Lyapunov to evaluate the divergence of nearby trajectories instead of considering neighbouring points remains to be carried out.

Apart from cross-links between our approach and covariant Lyapunov vectors, as discussed in Supplement D, there might also exist important connections to Lyapunov modes in interacting many-particle systems, see Ref. [32] for a short review and further references therein as well as Refs. [21,23]. Lyapunov modes refer to the eigenmodes associated with the spectrum of Lyapunov exponents which are closest to zero, projected onto the single particles from which they originate. They were found to form interesting spatio-temporal periodic patterns. The methods developed in our paper, based on solving the eigenvalue problem for the local symmetric Jacobian in a suitable local coordinate system, could possibly serve for developing alternative

techniques of computing such Lyapunov modes. Using our methods, it might also be interesting to check for spatio-temporal structures in the corresponding distribution of local Lyapunov exponents in such systems.

Some final remarks: Why reducing the tangent space (i.e. the points within a sphere) to points in a subspace orthogonal to the flow? Each point within the sphere is on a trajectory that has a reference point in the orthogonal subspace. Since the challenge is to find the trajectory which has the largest global separation, it seems sensible to use only orthogonal reference points. Then the local exponents already assess directly these neighbouring trajectories. If only global values are of interest, the established methods serve their purposes. However, if the interest includes more specifically also local properties as 'where and when the chaos starts', the analysis of short time intervals, transients, and more complex problems with coefficients changing in time, the 'constrained' RK method appears to be very useful. The results of this method can then, in turn, be approximated by evaluating the local extreme exponents using the orthogonal submatrix of the symmetric Jacobian for local Lyapunov exponents.

Acknowledgements

F.W. would like to thank P.F. Meier, H.R. Moser, and E.P. Stoll for valuable help. Both authors are grateful to Wm.G. Hoover and F. Grond for comments and for pointing out the important Refs. [11,15,21] to them. We also thank our reviewers for very helpful comments..

References

[1] A.M. Lyapunov, doctoral dissertation on stability of motion, St. Petersburg (Russian) (1892), Ann. Faculté des sciences, Université de Toulouse, 2 ser. (1907), Ann. Math. Study 17 (1977) (Princeton).

[2] V.I. Oseledec, A multiplicative ergodic theorem, Lyapunov characteristic numbers for dynamical systems, Trudy Moscow Mat. Obsc. 19 (1968) 179-210. English translation Trans. Moscow Math. Soc. 19 (1968) 197-221.

[3] G. Benettin, L. Galgani and J-M. Strelcyn, Kolmogorov entropy and numerical experiments, Phys. Rev. A 14 (1976) 2338-2345.

[4] J.D. Farmer, E. Ott, and J.A Yorke, The dimension of chaotic attractors, Physica 7D (1983) 153-180.

[5] A. Wolf, J.B. Swift, H.L. Swinney and J.A. Vastano, Determining Lyapunov exponents from a time series, Physica 16D (1985) 285-317.

[6] I. Goldhirsch, P.-L. Sulem, and S.A. Orszag, Stability and Lyapunov stability of dynamical systems: a differential approach and a numerical method, Physica 27D (1987) 311-337.

[7] J. M. Greene and J.-S. Kim, The calculation of Lyapunov spectra, Physica 24D (1987) 213-225.

[8] J.P. Eckmann and D. Ruelle, Ergodic theory of chaos and strange attractors, Rev. Mod. Phys. 57 (1985) 617-656.

[9] Ch. Skokos, The Lyapunov characteristic exponents and their computation, Lect. Notes Phys. 790 (2010) 63-135.

[10] K. Rateitschak and R. Klages, Lyapunov instability for a periodic Lorentz gas thermostated by deterministic scattering, Phys. Rev. E **65** (2002) 036209/1-11.

[11] F. Grond, H.H. Diebner, S. Sahle, A. Mathias, S Fischer, O.E. Rossler, A robust, locally interpretable algorithm for Lyapunov exponents, Chaos, Solitons and Fractals 16 (2003) 841-852.

[12] B. Eckhardt and D. Wintgen, Indices in classical mechanics. J. Phys. A: Math. Gen. 24 (1991) 4335-4348.

[13] P. Gaspard, Chaos, Scattering and Statistical Mechanics, Cambridge Nonlinear Science Series (No.9) Cambridge 1998, 1-495.

[14] Ch. Dellago and Wm. G. Hoover, Are local Lyapunov exponents continuous in phase space? Phys. Lett. A 268 (2000) 330-334.

[15] F. Grond, H.H. Diebner, Local Lyapunov exponents for dissipative continuous systems, Chaos, Solitons and Fractals 23 (2005) 1809-1817.

[16] H. Bosetti, H.A. Posch, C. Dellago and W.G. Hoover, Time-reversal symmetry and covariant Lyapunov vectors for simple particle models in and out of thermal equilibrium, Phys. Rev. E 82 (2010), 046218/1-10.

[17] E.N. Lorenz, Deterministic nonperiodic flow, J. Atmos. Sci. 230 (1963) 130-141.

[18] O.E. Rössler, An equation for hyperchaos, Phys. Lett. 71A (1979) 155.

[19] F. Ginelli, P. Poggi, A. Turchi, H. Chaté, R. Livi, A. Politi, Characterizing Dynamics with Covariant Lyapunov Vectors, Phys. Rev. Letters 99 (2007) 130601/1-4.

[20] I.G. Szendro, D. Pazo, M.A. Rodriguez and J.M. Lopez, Spatiotemporal structure of Lyapunov vectors in chaotic coupled-map lattices, Phys. Rev. E 76 (2007) 025202(R)/1-4.

[21] H. Bosetti, H.A. Posch, Covariant Lyapunov vectors for rigid disk systems, Chem. Phys. 375 (2010), 296-308.

[22] Wm.G. Hoover, C.G. Hoover, Local Gram-Schmidt and covariant Lyapunov vectors and exponents for three harmonic oscillator problems, Commun. Nonlinear Sci. Simulat. (2011), doi:10.1016/j.cnsns.2011.06.025.

[23] H.L. Yang and G. Radons, Comparison between covariant and orthogonal Lyapunov vectors, Phys. Rev. E 82 (2010), 046204/1-12.

[24] F. Waldner and R. Klages, Jacobian deformation ellipsoid and Lyapunov stability analysis revisited, arXiv:1008.0669.

[25] S.V. Ershov and A.B. Potapov, On the concept of stationary Lyapunov basis, Physica D 118 (1998), 167-198.

[26] C.G.J. Jacobi (1830), Gesammelte Werke, 7 vol., G. Reimer, Berlin (1881-1889).

[27] Wm.G. Hoover, C.G. Hoover, F. Grond, Phase-space growth rates, local Lyapunov spectra, and symmetry breaking for time-reversible dissipative oscillators, Communications in Nonlinear Scinece and Numerical Simulation 13 (2008) 1180-1193.

[28] E. Fick, Einführung in die Grundlagen der Quantentheorie. Aula-Verlag, Wiesbaden, 6th edition (1988), p.1-489.

[29] F. Waldner, Direct evaluation of local deformation tensor with Jacobi matrix – Lyapunov exponents orthogonal and parallel to flow well suited for transient chaos, Swiss Physical Society, Jahrestagung in Basel 20.-21. März 2003, 413.

[30] H.R. Moser and P.F. Meier, The structure of a Lyapunov spectrum can be determined locally, Phys. Lett. A 263 (1999) 167-174.

[31] K.E. Chlouverakis, A. Argyris, A. Bogris, and D. Syvridis, Complexity and synchronization in chaotic fiber-optic systems, Physica D 237 (2008) 568-572, and ref. therein.

[32] R. Klages, Microscopic Chaos, Fractals and Transport in Nonequilibrium Statistical Mechanics, Advanced Series in Nonlinear Dynamics (Vol. 24), World Scientific, Singapore, 2007, 1-441.

Figure Captions

Fig. 1. Lorenz chaos: Difference of the angles between the maximal expansion direction in a local frame flipped at time t=6.8 and the respective direction in the unflipped frame vs. time t. Above: free frame $\boldsymbol{V}$ of O [3]; Below: constraint frame $\boldsymbol{W}$ of RK [10] exhibiting a much shorter recovery time.

Fig. 2. Lorenz chaos: Local exponents vs. time t. Bottom: x-component. Top *left*: first exponent λ_{V1} (thick line); main extreme exponent α_1 (thin line). *Right*. first exponent λ_{W1} and extreme local separation $\beta_{\perp 1}$ orthogonal to flow (nearly same values). Second row: *Left*: Difference (λ_{V1}- α_1); *right:* difference ($\lambda_{\perp W1}$- $\beta_{\perp 1}$) at the same scale as left side. Third row: thin line: main extreme exponent α_1 *Left*: second exponent λ_{V2}; *right*: second exponent λ_{W2}= $\lambda_{\parallel W}$= $\varphi_{\parallel}$ acceleration along the flow. Note: Both local exponents λ_{V1} and λ_{V2} *(left)* consist of a mixing of separation $\lambda_{\perp W1}$ and acceleration $\lambda_{\parallel W}$ *(right)*.

Fig. 3. Lorenz chaos: Top left: angle between first vector $\underline{v}_1$ of the 'free' $\boldsymbol{V}$ frame and flow direction $\underline{f}_{\parallel}$ vs. x component. Top right: angle between direction $\underline{w}_{\perp 1}$ of the 'constrained' $\boldsymbol{W}$ frame ($\underline{w}_{\perp}$ always orthogonal to flow direction $\underline{f}_{\parallel}$) and direction $\underline{b}_{\perp 1}$ of the extreme separation exponent $\beta_{\perp 1}$ vs. x component. Bottom right: exponent $\lambda_{\perp W1}$ vs. extreme separation exponent $\beta_{\perp 1}$ Straight diagonal line: limit $\lambda_{\perp W1}$ = $\beta_{\perp 1}$. Bottom left: first 'free' exponent λ_{V1} vs. $\beta_{\perp 1}$, similar straight line λ_{V1} =$\beta_{\perp 1}$.

Fig. 4. Lorenz chaos: Projection of the trajectory at equal time intervals onto the yz-plane when the local exponents exceed c = 4. Left: 'free' case, right: 'constrained case. Top: maximum exponent α_1 and maximum separation exponent $\beta_{\perp 1}$. Centre: first exponent $\lambda_{\perp V1}$ and $\lambda_{\perp W1}$; bottom: second exponent λ_{V2} and $\lambda_{\parallel W}$= $\varphi_{\parallel}$, respectively.

Fig. 5. Lorenz model: chaotic transient to an attracting fixed point for control parameters (σ, ρ, b)=(16, 28.165, 4). Trajectories are projected onto the yz plane at equal time intervals to indicate the changes in velocity. The line indicates the position of the Poincaré plane z=c_p=const. with c_p=27.165 through the fixed points. Local exponents are integrated over each time interval between consecutive Poincaré points.

Fig. 6. Lorenz 'chaotic transient to a fixed point'; Bottom: $x(t)$. Centre: Angle of the first axis of the $\boldsymbol{V}$ frame relative to the flow direction. The $\boldsymbol{V}$ frame is *artificially* rotated by 90 degrees at t = 7. Top: Poincaré

integrals of the first two exponents of the ***V*** frame denoted by the symbols o and +, respectively. Lines are only guides to the eye. Note the 'artificial bump' between $t \approx 22$ and 27 as explained in the text.

Fig. 7. Lorenz 'chaotic transient to a fixed point'; Bottom: $x(t)$. Centre: Angle between the first orthogonal direction of the ***W*** frame and the direction of the local orthogonal direction of extreme separation. The ***W*** frame is artificially rotated by 90 degrees at $t = 7$. Top: Poincaré integrals of the first two exponents of the ***W*** frame denoted by the symbols o and +, respectively. The dots plotted above the o symbols are the integrals of the local extreme orthogonal exponents, which are independent of orientation and flipping of the ***W*** frame.

Table Caption

Table 1. Illustration of the relations between the elements in the four local frames. Note that the parallel exponents of 1.2. and 2.2. are equal and both need no integration.

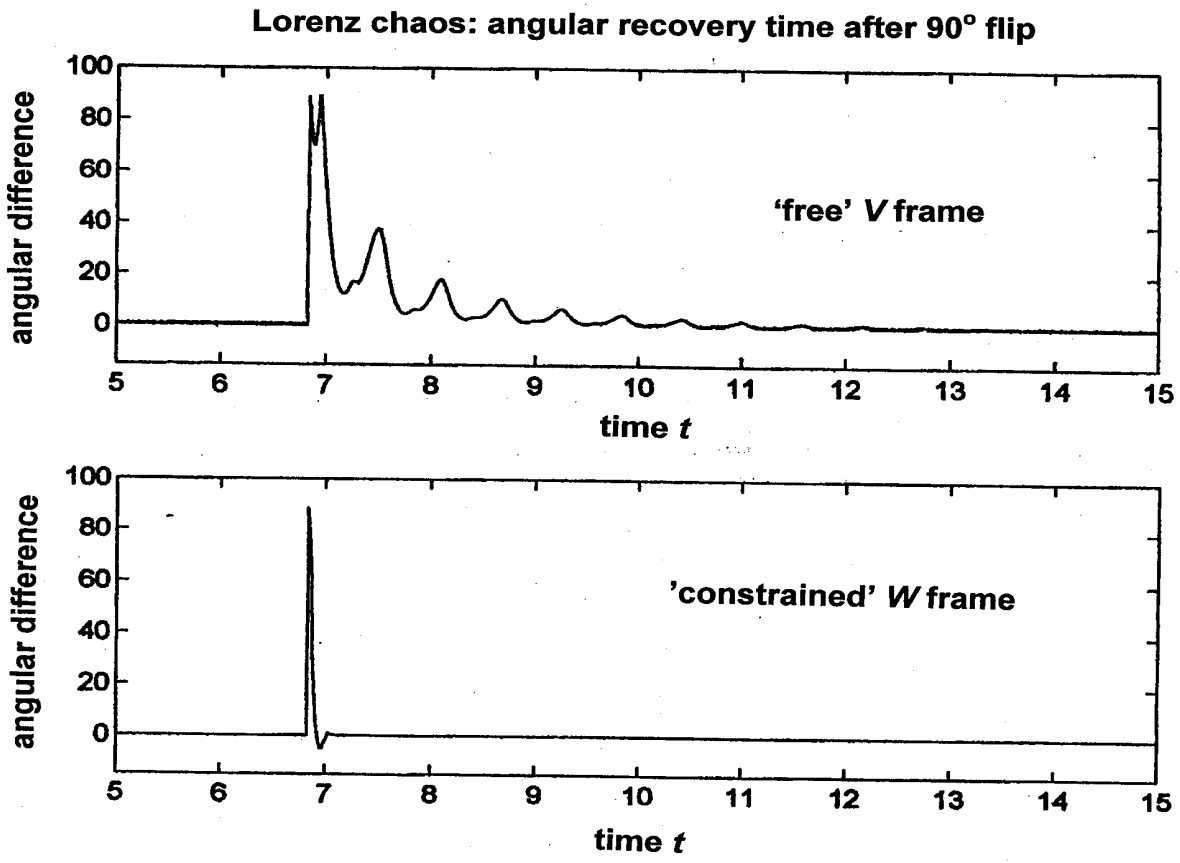
Lorenz chaos: angular recovery time after 90° flip
angular difference
100
80
60
40
20
0
5
6
7
8
9
10
11
12
13
14
15
time t
'free' V frame
angular difference
'constrained' W frame
time t

Fig. 1

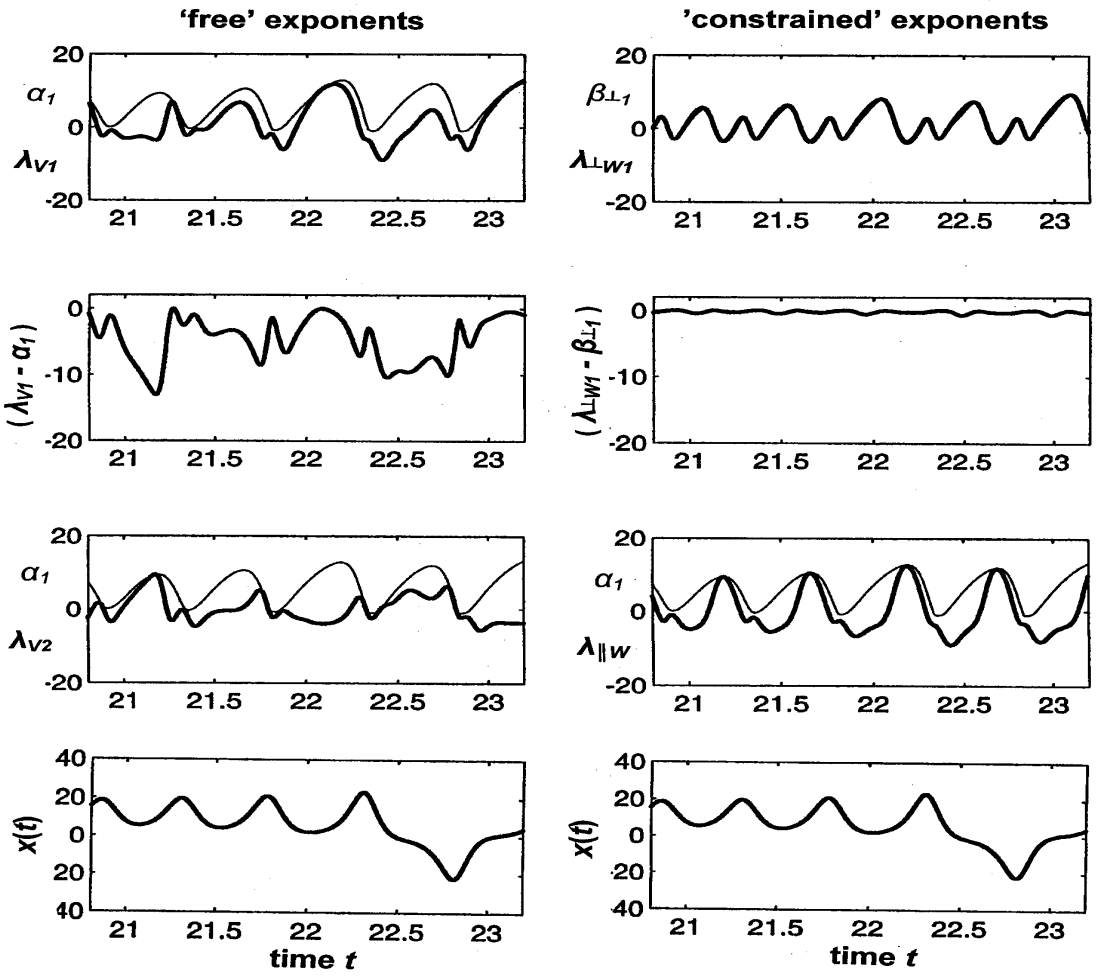
'free' exponents
'constrained' exponents
α_1
λ_{V1}
$\beta_{\perp 1}$
$\lambda_{\perp W1}$
$(\lambda_{V1} - \alpha_1)$
$(\lambda_{\perp W1} - \beta_{\perp 1})$
α_1
λ_{V2}
α_1
$\lambda_{\parallel W}$
x(t)
x(t)
time t
time t

Fig. 2

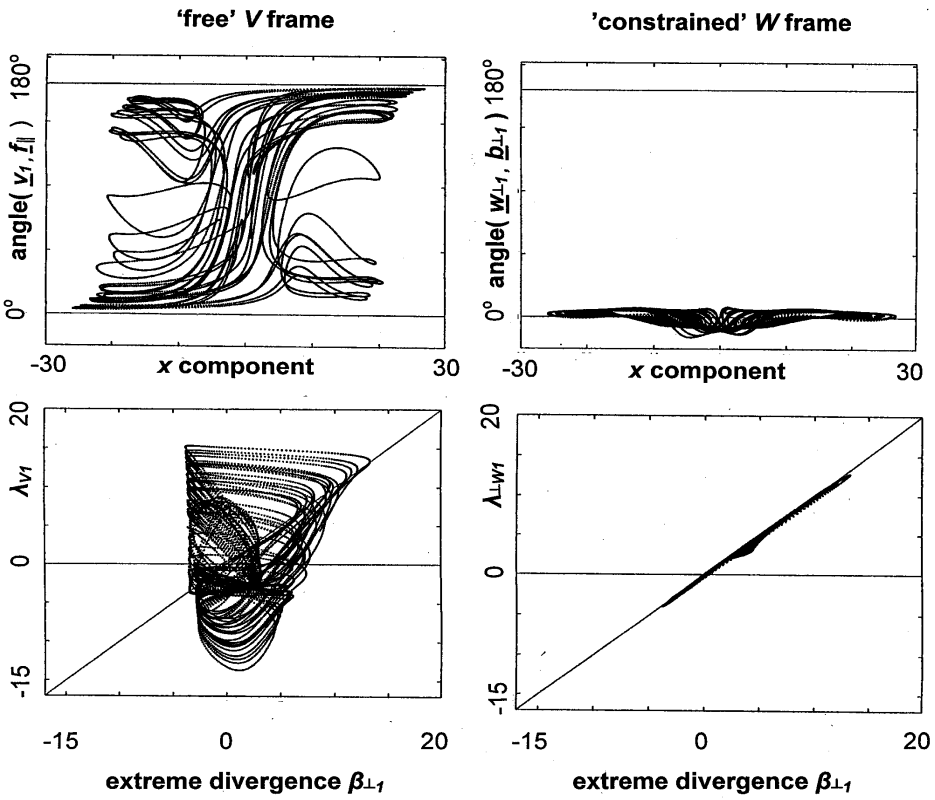
'free' V frame
'constrained' W frame
0° angle(v1, f||) 180°
0° angle(w⊥1, b⊥1) 180°
-30
x component
30
λV1
λ⊥W1
20
0
-15
extreme divergence β⊥1

Fig. 3

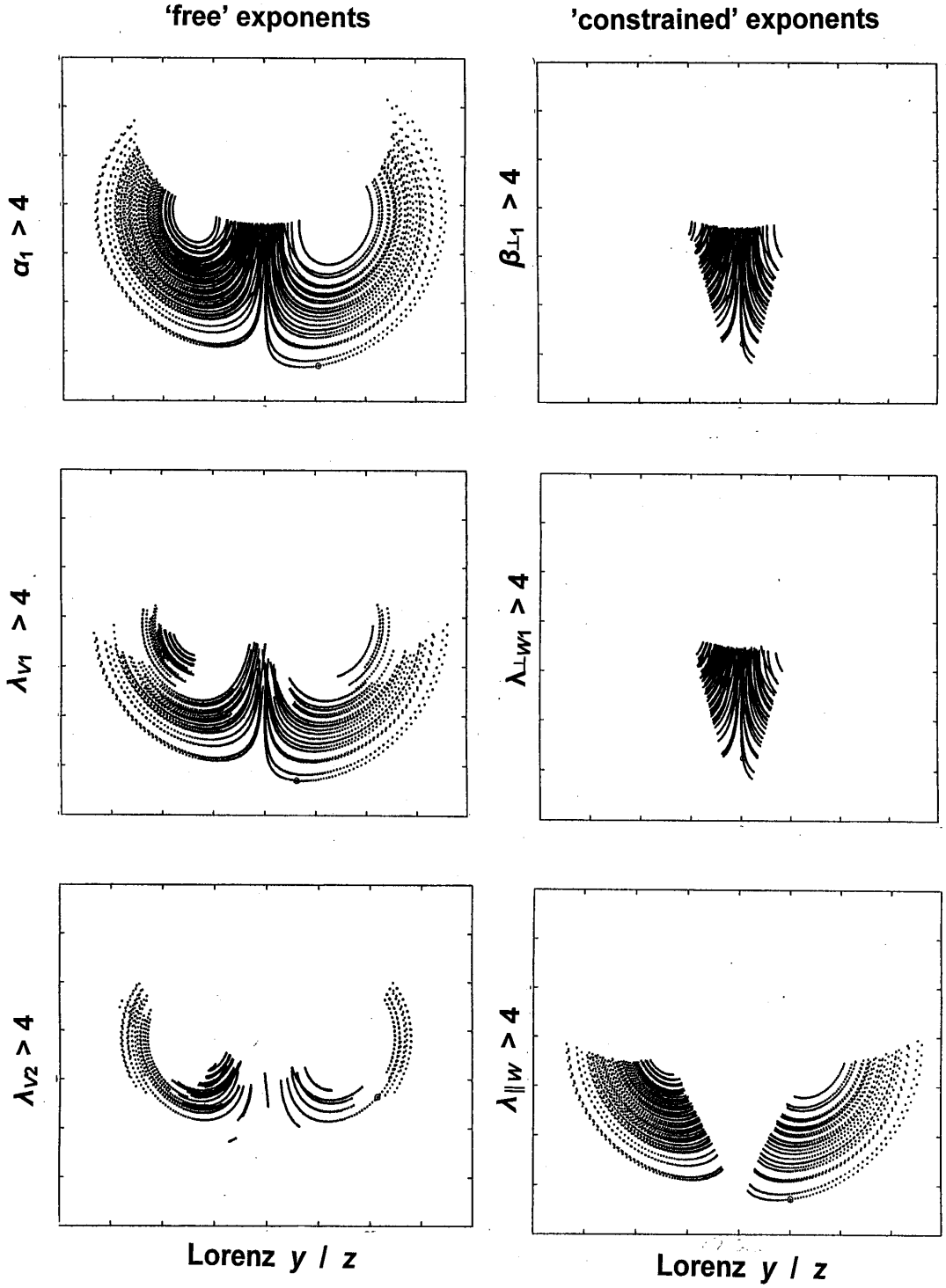
'free' exponents
'constrained' exponents
$\alpha_1 > 4$
$\beta_{\perp 1} > 4$
$\lambda_{v1} > 4$
$\lambda_{\perp w1} > 4$
$\lambda_{v2} > 4$
$\lambda_{\parallel w} > 4$
Lorenz y / z
Lorenz y / z

Fig. 4

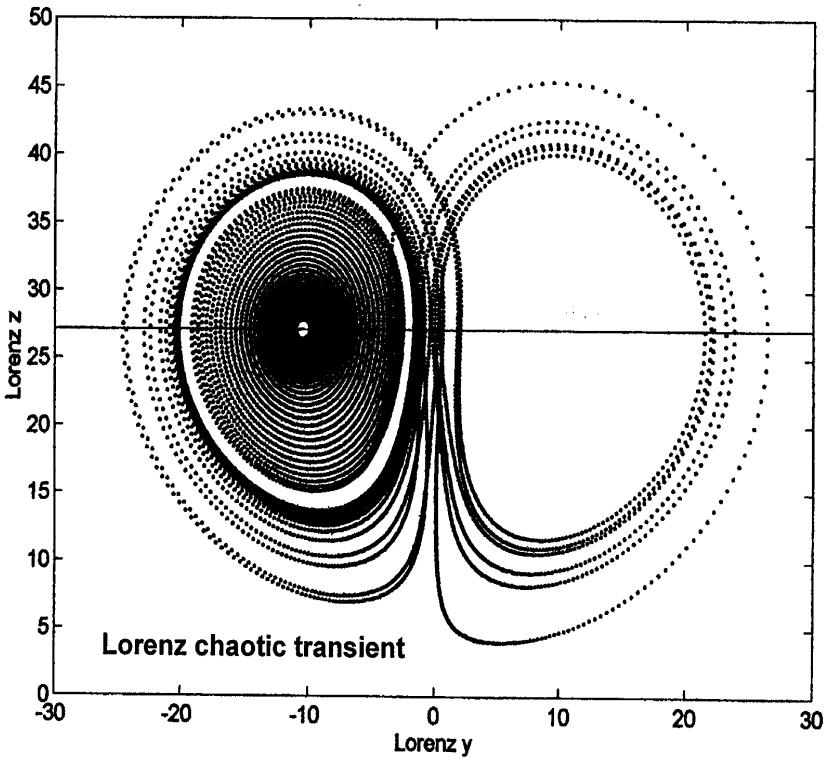
Lorenz chaotic transient
Lorenz z
Lorenz y
50
45
40
35
30
25
20
15
10
5
0
-30
-20
-10
0
10
20
30

Fig. 5

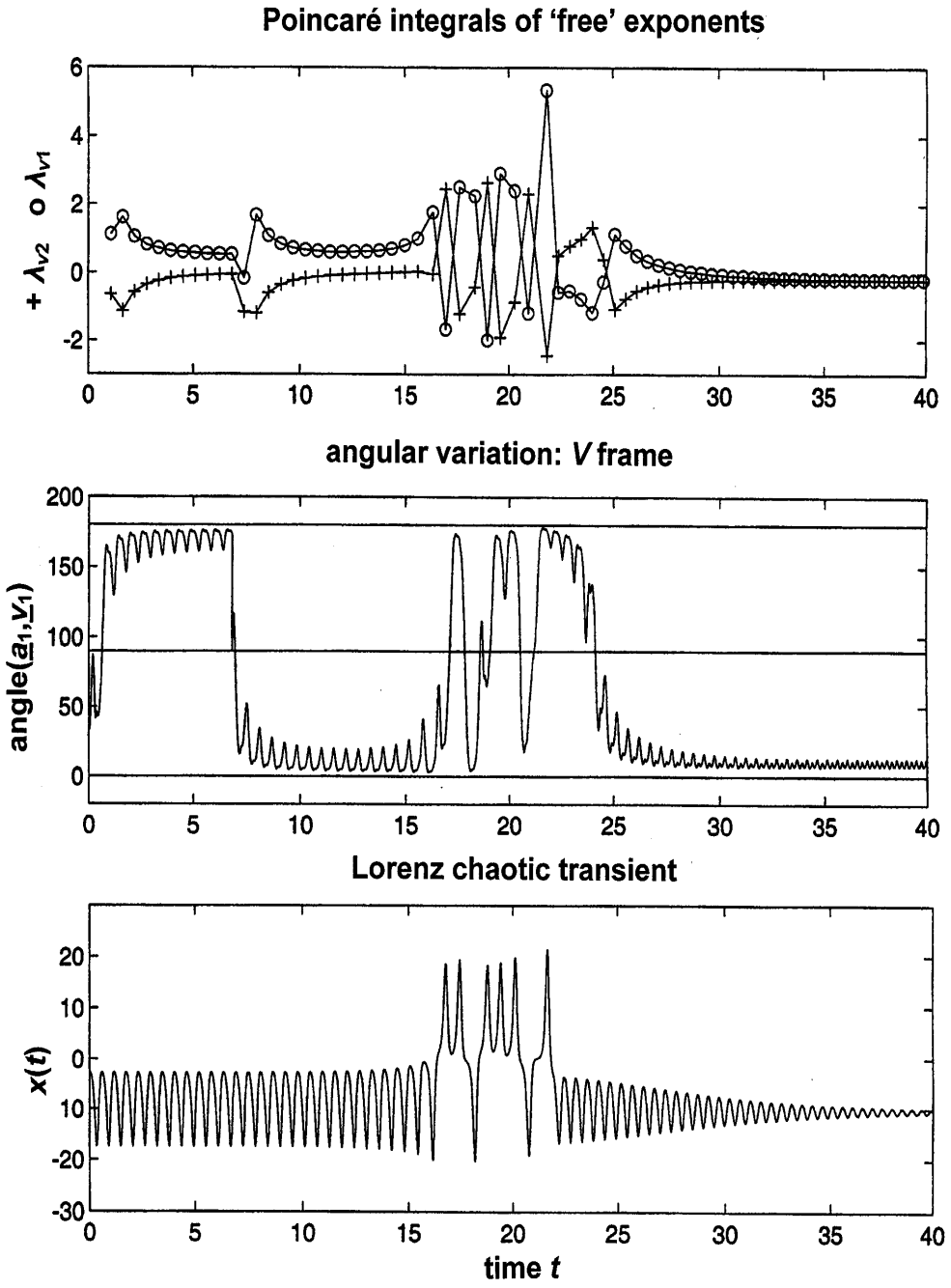
Poincaré integrals of 'free' exponents
+ λv2 o λv1
angular variation: V frame
angle(a1,v1)
Lorenz chaotic transient
x(t)
time t

Fig. 6

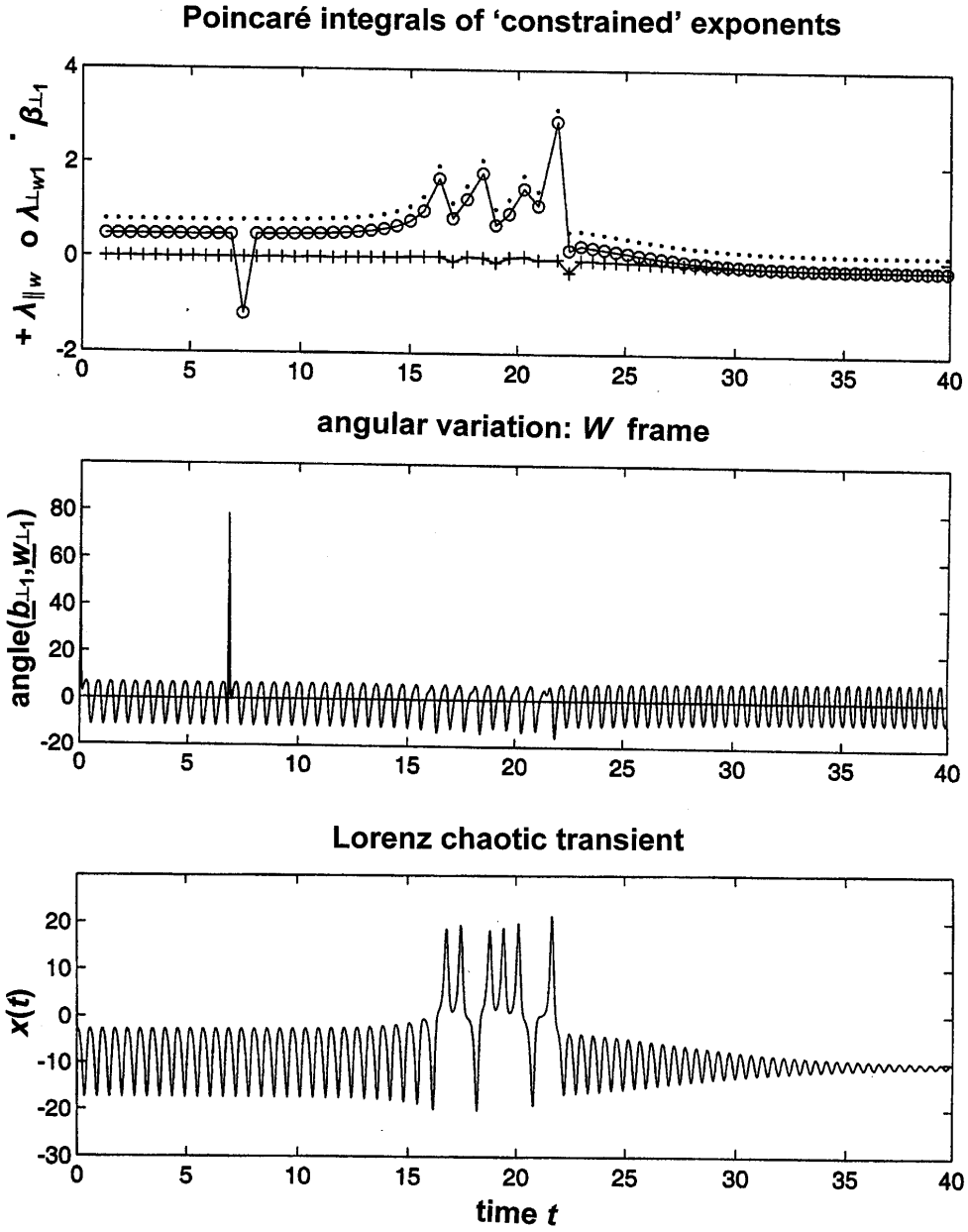
Poincaré integrals of 'constrained' exponents
$+\lambda_{\|w}$ o $\lambda_{\perp w1}$. $\beta_{\perp 1}$
4
2
0
-2
0 5 10 15 20 25 30 35 40
angular variation: W frame
angle($\underline{b}_{\perp 1}$,$\underline{w}_{\perp 1}$)
80
60
40
20
0
-20
0 5 10 15 20 25 30 35 40
Lorenz chaotic transient
x(t)
20
10
0
-10
-20
-30
0 5 10 15 20 25 30 35 40
time t

Fig. 7

	free 'full'	**constrained** $\parallel$ and 'reduced' $\perp$ to d$\underline{x}$ $\parallel$ $\underline{f}_{\parallel}$	
strictly local for all points $\underline{x}$ in phase space no integration	1.1. $\boldsymbol{A}$ $\underline{a}_i$ α_i	1.2 $\boldsymbol{B}$ $\underline{b}_{\parallel}=\underline{f}_{\parallel}$, $\underline{b}_{\perp k}$ $\beta_{\parallel}=\varphi_{\parallel}$ and $\beta_{\perp k}$	**local extreme** matrix, unit vectors local exponents
local at $\underline{x}(t)$, but after integration along trajectory $\{\underline{x}(t_k)\}$ k=0…n	2.1 $\boldsymbol{V}$ $\underline{v}_i$ λ_{Vi}	2.2 $\boldsymbol{W}$ $\underline{w}_{\parallel}=\underline{f}_{\parallel}$, $\underline{w}_{\perp k}$ $\lambda_{\parallel W}=\varphi_{\parallel}$ and $\lambda_{\perp Wk}$	**local 'unique'** matrix, unit vectors local exponents

Table 1